EFFECT OF DIELECTRIC SUBSTRATE ON RADIATION FROM MICROSTRIP ANTENNAS

A Thesis Submitted
in Partial Fulfilment of the Requirements
for the Degree of
MASTER OF TECHNOLOGY

By

ANUP KUMAR GOGOI

to the
DEPARTMENT OF ELECTICAL ENGINEERING
INDIAN INSTITUTE OF TECHNOLOGY, KANPUR
AUGUST, 1981

EE-1981-M-GOG-EFF

C E R T I F I C A T E

This is to certify that the work reported in this thesis entitled 'EFFECT OF DIELECTRIC SUBSTRATE ON RADIATION FROM MICROSTRIP ANTENNAS' by Mr. Anup Kumar Gogoi has been carried out under my supervision and has not been submitted elsewhere for a degree.

(K. C. GUPTA)
Professor
Department of Electrical Engineering
Indian Institute of Technology
Kanpur-208016
INDIA

ACKNOWLEDGEMENT

I express my deep sense of gratitude to Professor K.G. Gupta for his valuable guidance and the encouragement I received from him at every stage of this work.

I convey my thanks to Dr. Ramesh Garg, Asstt. Prof. I.I.T. Kharagpur, for many fruitful discussions with him during his stay at I.I.T. Kanpur.

I extend my heartfelt thanks to all my friends for their cooperation and nice company.

Thanks are due to Mr. Yogendra Chandra for efficient typing and Mr. S.K. Bajpayee for neat drawings.

Aug. 1981 ANUP KUMAR GOGOI

ABSTRACT

These investigations are aimed at evaluating the effect of dielectric substrate on the radiation from microstrip antennas. Two approaches are considered. Firstly radiating edges of the microstrip antenna are modelled by line and sheet sources of magnetic current. Radiation from these magnetic current sources is evaluated by using steepest descent method in Fourier transform domain. The second approach is based on Weiner-Hopf techniques. A dielectric filled planar waveguide with top conductor truncated at z=0 is analyzed. Reflection coefficient and radiation pattern are calculated. Edge resistance and equivalent extension of periphery to account for fringing field is calculated therefrom.

TABLE OF CONTENTS

CHAPTER 1

INTRODUCTION

1.1 Microstrip Antennas:

Microstrip antennas are used in various communication systems[1]. One basic form of microstrip antennas is shown in Fig. 1.1. It consist of a rectangular conducting patch in one side of the dielectric substrate backed by a ground plane on the other side. Several other configuration as circular, triangular, ring type etc are also used[1].

To study radiation from microstrip antennas, the rectangular configuration shown in Fig. 1.2 may be considered. The cross sectional view of the antenna is shown in Fig. 1.3. The spacing between the conducting patch and the ground plane being only a small fraction of the wavelength, the electric field can be assumed to be constant along the height of the antenna. The field variation along the length of the antenna is shown in Fig. 1.3. The length 'L' is very nearly equal to $\lambda_g/2$, where λ_g is the effective wave length in the dielectric medium. The field may vary also along the width depending on the position of feed point(and the frequency of operation). Radiation takes place from the fringing fields which are present at the aperture formed by the boundary of the patch conductor and the ground plane.

An aperture approach was used by James and Wilson[2] to approximate the radiation fields of a microstrip antenna. In this approach, the total field in a aperture is considered to be sum of an incoming TEM wave and the reflected field at the edge of the radiating patch. If the reflection coefficient is accurately known, the field distribution in the aperture can be precisely determined. Even in absence of exact aperture field distribution, this approach yields a resonably good approximation of the fields.

Lo et al.[3] have modelled microstrip antennas as cavities. The method based on the fact that the tangential magnetic field along the periphery of the aperture is negligibly small. The electric field between the ground plane and the patch boundary can be represented as magnetic current sheet. Thus the microstrip structure can be considered as a cavity which has two parallel conducting plates bounded by a magnetic side walls. The magnetic current sheet around the periphery and its image on the ground plane is used to compute radiation fields.

Carver and Coffey[4] have advanced a similar model which also considers a microstrip antenna as a resonant cavity. Modal expansion technique is used to find field inside the cavity. The main difference between the two

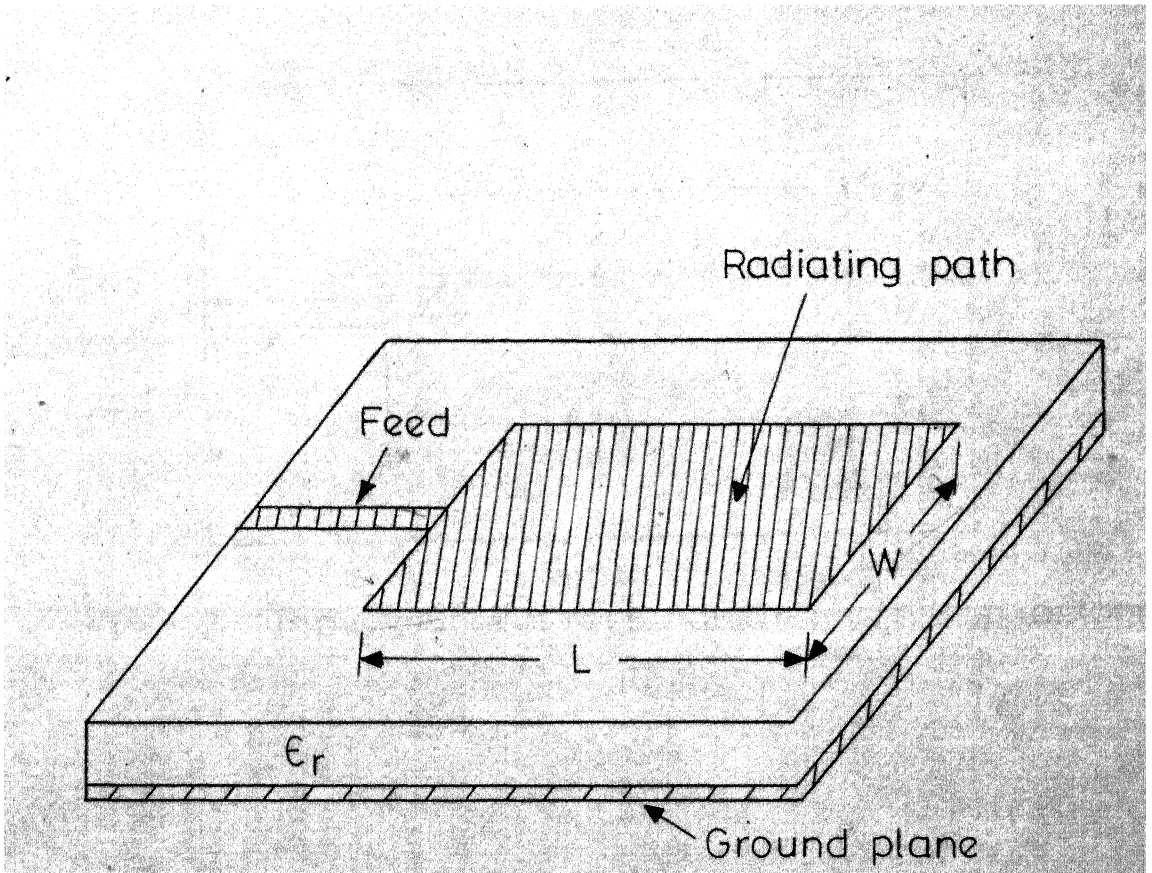

Fig. 1.1 A rectangular microstrip antenna.

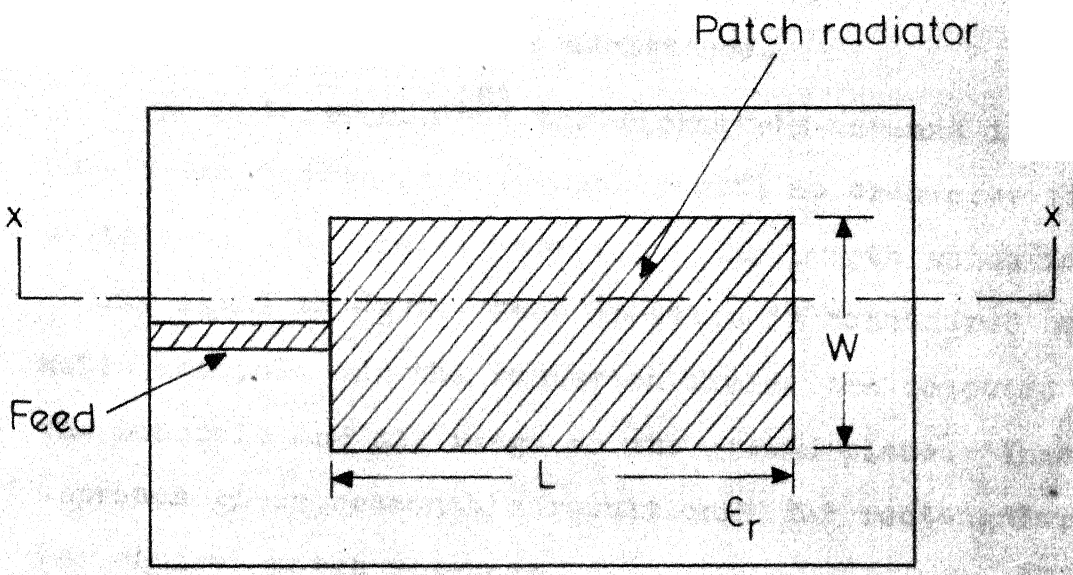

Fig.1.2 Top view of a rectangular microstrip antenna.

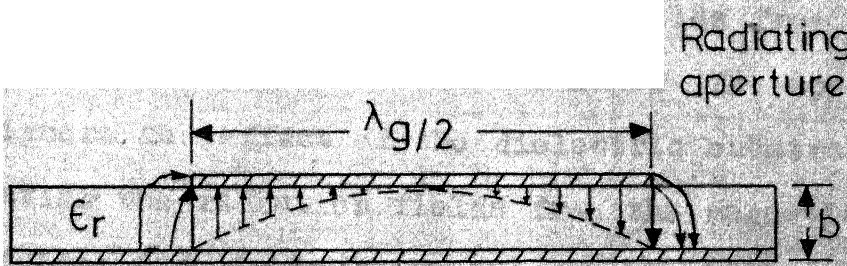

Fig.1.3 Sectional view of a microstrip antenna with E lines (cutting plane x-x).

models is in the application of boundary conditions on the boundary wall. In this model the boundary wall is allowed to have a complex admittance.

In another model[5] the microstrip antenna is treated as a transmission line resonatar with no tranverse field variation. The fields vary along the length which is very nearly equal to $\lambda g/2$. Each aperture is considered as magnetic monopole and the radiation fields are computed from the monopole and its image on the ground plane. This approach gives reasonable result only for rectangular (or square) patch antennas.

1.2 Present Investigation:

In the methods described above, an approximation is made while calculating the radiation fields from the computed magnetic current distributions. The approximation is to ignore the effect of the dielectric substrate while calculating the radiation fields from the magnetic current distribution and its image on the ground plane. The main aim of the present study is to investigate the validity of this approximation. A single radiating slot is considered for studying the effect of dielectric substrate on the radiation from microstrip antennas. Using Kirchoffs-Huygen's principle the fringing electric field may be exp-

ressed as magnetic current distribution.

In Chapter Two, a radiating aperture is modelled as a magnetic current sheet (Fig. 2.2). The current distribution being present inside the dielectric substrate. An expression for radiation fields for a line current source inside the dielectric (Fig. 2.1) is derived. Using superposition principle radiation field from the current sheet is obtained. The approach is used also for studying a horizontal current sheet placed on the dielectric substrate (Fig. 2.3).

Chapter Three describes another approach for study of microstrip antennas. The edge of a parallel plate wave guide where one plate is truncated abruptly (Fig. 3.1) can be considered to be a radiating aperture of a microstrip antenna. TEM wave is assumed to be pragating towards this edge inside the wave guide. The calculated reflected field may be used to compute edge admittance of the structure. The Weiner-Hapf technique is used for this purpose. The extent of fringing field outside the wave guide and outward extension of the boundary in the planar resonator model is also computed from this analysis.

Chapter Four summarizes the main results and suggests the possible extension of these investigations.

CHAPTER 2

RADIATION FROM MAGNETIC CURRENT SOURCES ON A GROUNDED DIELECTRIC SUBSTRATE

In this chapter, radiation fields for three types of magnetic current sources within (or on) a grounded dielectric substrate are derived. The three current sources considered are (i) a line current within the dielectric, (ii) a vertical current sheet inside the dielectric and (iii) a horizental current sheet on the top surface of the substrate. Fourier transform technique is used for solving the inhomogenous wave equations encountered in this analysis. The resultant contour integration obtained is evaluated by steepest descent method for the far field.

2.1 A Line Current Source Inside the Substrate

2.1.1 Formulation of the Problem:

Consider a dielectric substrate with height b and dielectric constant ε_r, with a perfectly conducting ground plane on one side as shown in Fig. 2.1 . The substrate extends to infinity in both y and z directions. There is a line source of magnetic current at $x = a$, $z = 0$. Due to lateral uniformity of the structure, there is no variation of field in y direction. Thus $\partial/\partial_y = 0$ and the electromagnetic fields have only three non-zero components, H_y, E_x

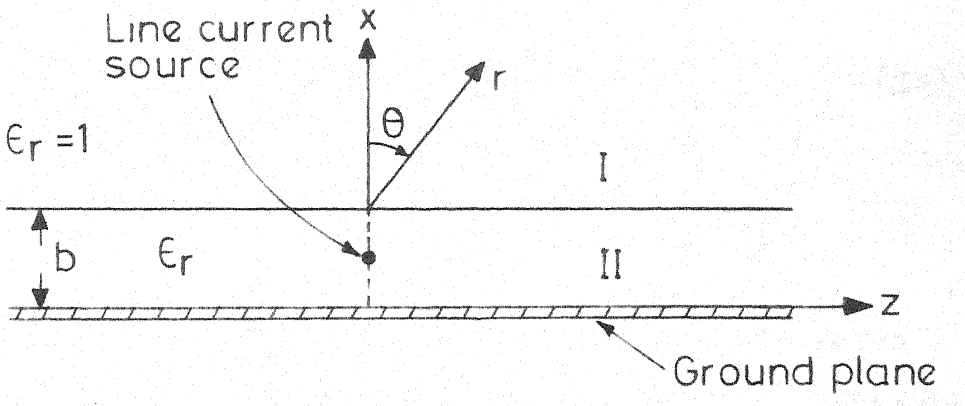

Fig . 2.1 A line current soure inside the substrate .

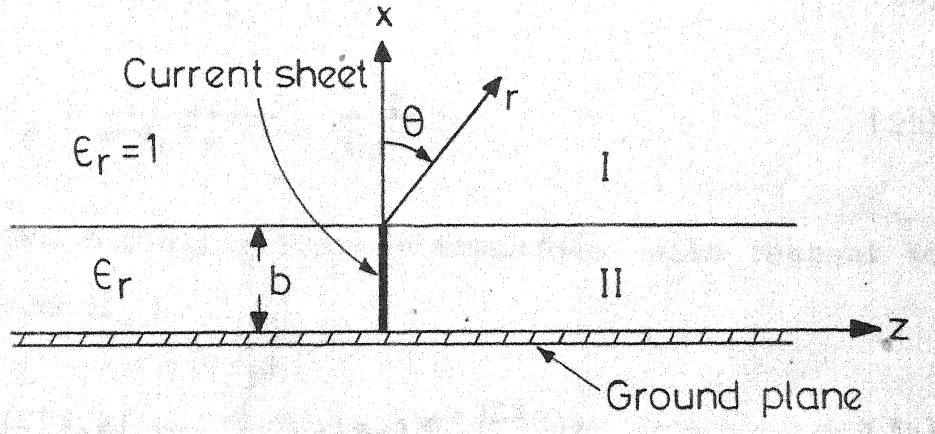

Fig. 2.2 A vertical current sheet inside the dielectric substrate .

and E_z ($H_x=H_z=E_y=0$). H-fields in regions I and II satisfy the following two equations respectively.

$$(\nabla_T^2 + \omega^2\mu\varepsilon)H_{y1} = 0 \qquad (1a)$$

$$(\nabla_T^2 + \omega^2\mu\varepsilon_o\varepsilon_r) H_{y2} = -j\omega\varepsilon_o\varepsilon_r\,\delta(x-b)\delta(z) \qquad (1b)$$

Where $\nabla_T^2 = \frac{\partial^2}{\partial x^2} + \frac{\partial^2}{\partial z^2}$, and δ denotes Dirac's delta function. Time variation is taken as $e^{-j\omega t}$. Subscript 1 and 2 correspond to fields in region I and II respectively. The other field components are given by the following relation:

$$E_x = \frac{1}{j\omega\varepsilon_o\varepsilon_r}\left(\frac{\partial H_y}{\partial z}\right) \qquad (2a)$$

$$E_z = \frac{j}{\omega\varepsilon_o\varepsilon_r}\left(\frac{\partial H_y}{\partial x}\right) \qquad (2b)$$

The following Fourier transforms with respect to z are introduced.

$$\Psi_1(x,\beta) = \int_{-\infty}^{\infty} H_{y1}(x,z)e^{-j\beta z}\,dz \qquad (3a)$$

$$H_{y1} = \frac{1}{2\pi}\int_{-\infty}^{\infty} \Psi_1(x,\beta)e^{j\beta z}\,d\beta \qquad (3b)$$

$$\Psi_2(x,\beta) = \int_{-\infty}^{\infty} H_{y2}(x,z)e^{-j\beta z}\,dz \qquad (3c)$$

$$H_{y2}(x,z) = \frac{1}{2\pi}\int_{-\infty}^{\infty} \Psi_2(x,\beta)e^{j\beta z}\,d\beta \qquad (3d)$$

Taking Fourier transforms of eqns (1a) and (1b) ... two ordinary differential equations are obtained. These differential equations are to be solved in the transform domain (x,β plane) with the transformed boundary conditions. Inverse transform yields the desired field. Taking Fourier transform of eqn.(1a) and (1b), one gets,

$$\frac{d^2\Psi_1}{dx^2} - h_o^2\Psi_1 = 0 \qquad x \geqslant b \qquad (4a)$$

$$\frac{d^2\Psi_2}{dx^2} + h_1^2\Psi_2 = -j\omega\varepsilon_o\varepsilon_r\delta(x-a) \qquad 0 \leqslant x \leqslant b \qquad (4b)$$

where $h_o = \sqrt{(\beta^2 - k_o^2)}$ (5a)

$h_1 = \sqrt{(k_o^2\varepsilon_r - \beta^2)}$ (5b)

k_o = free space propagation constant = $\omega\sqrt{\mu_o\varepsilon_o}$ (5c)

General solution to eqns (4a) and (4b) can be written

$$\Psi_1 = D e^{-h_0 x} + F e^{h_0 x} \qquad x \geq b \qquad (6a)$$

$$\Psi_2 = B \sin(h_1 x) + C \cos(h_1 x) \qquad a \leq x \leq b \qquad (6b)$$

$$\Psi_2 = A_1 \sin(h_1 x) + A_2 \cos(h_1 x) \qquad 0 \leq x \leq a \qquad (6c)$$

The set of simutaneous equations given by (6) are solved with the following boundary conditions.

Boundary Conditions

(a) The tangential component of magnetic field is continous at the air-dielectric interface x=b, i.e.

$H_{y1}(b^+, z) = H_{y2}(b^-, z)$

Using (3a) and (3c) one gets

$$\Psi_1(b^+, \alpha) = \Psi_2(b^-, \alpha) \qquad (7a)$$

(b) The tangential component of electric field is continous at the air-dielectric interface.

At $x=b$, $E_{z1}(b^+, z) = E_{z2}(b^-, z)$

Using (2b), (3a) and (3c) this boundary condition can be written in transformed domain as

$$\varepsilon_r \left.\frac{d\Psi_1}{dx}\right|_{x=b^+} = \left.\frac{d\Psi_2}{dx}\right|_{x=b^-} \qquad (7b)$$

(c) At $x=a$, ψ_2 is continous (7c)

(d) At $x=a$, $\left.\frac{d\psi_2}{dx}\right|_{x=a^+} - \left.\frac{d\psi_2}{dx}\right|_{x=a^-} = -j\omega\varepsilon_o\varepsilon_r$ (7d)

This is obtained by integrating (4b) from $x=a^-$ to a^+.

(e) Tangential electric field is zero at ground plane.

at $x=0$, $E_z = 0$

$$\left.\frac{d\psi_2}{dx}\right|_{x=0} = 0 \qquad (7e)$$

Proper branch of h_o should be such that it leads to outward propagating or attenuated waves. This requires F in (6a) to be zero. Boundary condition given by (7e) gives $A_1=0$ in (6c). The set of equations given by (6) can be written as

$$\psi_1 = De^{-h_o x} \qquad x \geqslant b \qquad (8a)$$

$$\psi_2 = B\,\mathrm{Sin}(h_1 x) + C\,\mathrm{Cos}(h_1 x) \qquad a \leqslant x \leqslant b \qquad (8b)$$

$$\psi_2 = A\,\mathrm{Cos}(h_1 x) \qquad 0 \leqslant x \leqslant a \qquad (8c)$$

Using (8) and the boundary conditions given by (7), the following set of simultaneous equations (written in the matrix form) is obtained.

$$\begin{bmatrix} \sin(h_1 a) & \cos(h_1 a) & -\sin(h_1 a) & 0 \\ -\cos(h_1 a) & \sin(h_1 a) & \cos(h_1 a) & 0 \\ 0 & \cos(h_1 b) & -\sin(h_1 b) & \frac{\varepsilon_o h_o}{h_1} e^{-h_o b} \\ 0 & \sin(h_1 b) & \cos(h_1 b) & -e^{-h_o b} \end{bmatrix} \begin{bmatrix} A \\ B \\ C \\ D \end{bmatrix} = \begin{bmatrix} -j\,\varepsilon_o \varepsilon_r / h_1 \\ 0 \\ 0 \\ 0 \end{bmatrix} \qquad (9)$$

Solving eqn. (9) for D, one gets,

$$D = \frac{-j\omega\varepsilon_o\varepsilon_r \cos(h_1 a)\, e^{h_o b}}{h_1 \sin(h_1 b) - \varepsilon_r h_o \cos(h_1 b)} \qquad (10)$$

Substituting D in (8a) from (10) and then taking the Inverse Fourier Transform, the field in the region x b can be obtained. The magnetic field H_{y1} is given by the following expression.

$$H_{y1}(x,z) = \frac{1}{2\pi}\int_{-\infty}^{\infty} D\, e^{-h_o x + j\beta z}\, d\beta \qquad (11)$$

where D is given by (10)

The integration in (11) cannot be carried out analytically. However, the far field can be approximated using steepest descent method. Appendix A describes the steepest decent method. The radiation field $H_{y1}(r, \theta)$ for the magnetic line current is given by the expression

$$H_{y1}(r,\theta) = -\omega\varepsilon_o\varepsilon_r\sqrt{\frac{1}{2\pi k_o r}}\; e^{j(k_o r-\pi/4)}\; f_1(\theta) \qquad (12a)$$

where $$f_1(\theta) = \frac{\cos\theta \cos(k_o ua)}{\varepsilon_r \cos\theta \cos(k_o ub) - ju \sin(k_o ub)} \qquad (12b)$$

$$u = \sqrt{(\varepsilon_r - \sin^2\theta)} \qquad (12c)$$

θ and r are cylindrical coordinates shown in Fig. (2.1).

The radiated power density in free space is proportional to the square of the field intensity. Total power (P) radiated from a unit length of the line source can be written as

$$P = 2\int_0^{\pi/2} \eta\left\{H_{y1}(r,\theta)\right\}^2 \, d\theta \qquad (13a)$$

where η is the intrinsic impedance of free space.

Radiation resistance is calculated from the knowledge of the radiated power for a given strength of the magnetic current source. Magnetic current is expressed in volts and thus, radiation resistance 'R_r' is obtained from the expression

$$R_r = \frac{\text{Power Radiated in Watts}}{\text{Strength of source in Volts}} \qquad (13b)$$

2.1.2 Numerical Results:

Radiation pattern for a line current source is shown in Fig. 2.5. The curves 1,2,3 and 4 are for the following cases, (operating frequency 3 GHz).

1. The source on the ground plane with ϵ_r=2.53 and b = 0.328 cm.
2. The source on the ground plane with ϵ_r=2.53 and b = 0.159 cm.
3. The source on the substrate with ϵ_r = 2.53 and b = 0.159 cm.
4. ϵ_r = 1 and the source position from the ground plane $\leq$ 0.328 cm.

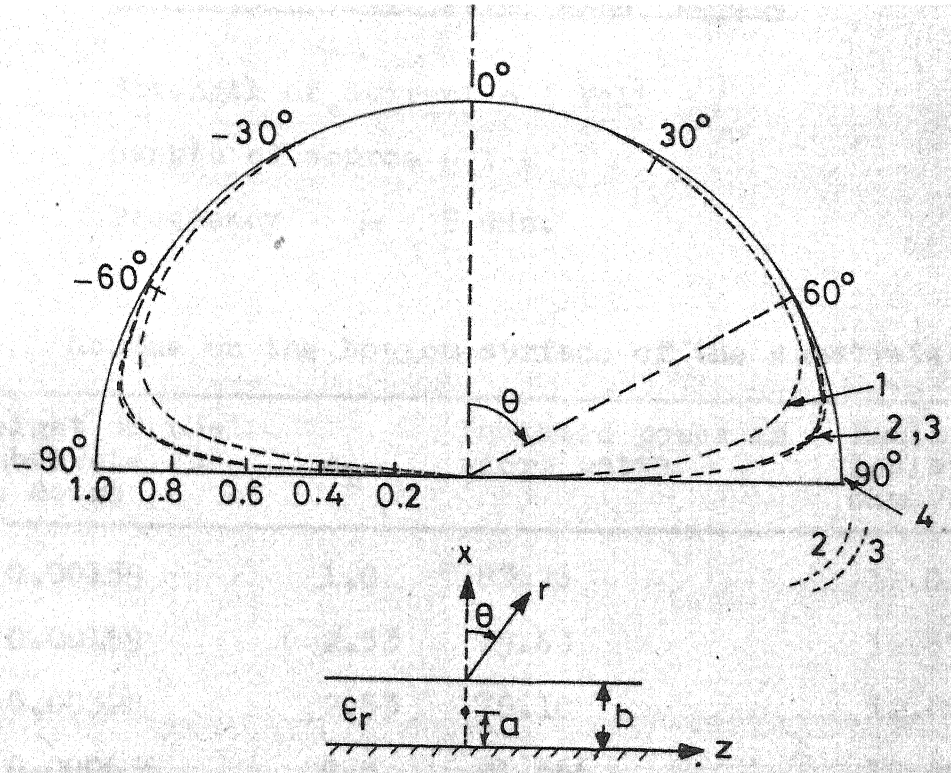

$\epsilon_r = 2.53$

Frequency 3 GHz

1. $\begin{cases} b = 0.328 \text{ cm} \\ a = 0 \\ \epsilon_r = 2.53 \end{cases}$

2. $\begin{cases} b = 0.159 \text{ cm} \\ a = 0 \\ \epsilon_r = 2.53 \end{cases}$

3. $\begin{cases} b = 0.159 \text{ cm} \\ a = b \\ \epsilon_r = 2.5 \end{cases}$

4. $\begin{cases} a = 0, a = b < 0.328 \text{ cm} \\ \epsilon_r = 1.0 \end{cases}$

Fig. 2.5 Radiation pattern for line current source ($|Hy|$ vs θ).

Table 2(a)

Radiated Power from Line Source

Strength of current = 1 Volt

Length of source = 1 m

Frequency = 3 GHz.

Source on the bottom surface of the substrate (a = 0)

Height of the substrate 'b' in metre	ε_r	Radiated power in micro watts	Radiation Resistance in ohms/metre
0.00159	1.0	83.26	12.010
0.00159	2.53	79.63	12.558
0.00328	2.53	78.10	12.804
0.000635	9.8	81.566	12.26

Source on the top surface of the substrate

Height of the substrate 'b' in metre	ε_r	Radiated power in micro watts	Radiation Resistance in ohms/metre
0.00159	1	82.84	12.071
0.00328	1	81.49	12.271
0.00159	2.53	77.80	12.853
0.00328	2.53	71.37	14.011
0.000635	9.8	80.362	12.443

When ε_r is increased the radiation pattern gets modified near end-fire direction. The deviation is more for a thicker substrate. By comparing radiation patterns 2 and 3 we note that radiation patterns for sources on the ground plane or on the substrate are quite similar. When the source is on the ground plane the radiation near end-fire direction is reduced little more than that of the case when the source is on top of the substrate.

The radiated power (for a unit source) and radiation resistance are tabulated in Table 2(a). Radiated power decreases when dielectric constant 'ε_r' or the height of the substrate 'b' is increased. An decrease in radiated power indicates an increase in radiation resistance.

2.2 A Vertical Current Sheet Inside the Substrate:

A radiating aperture in a microstrip antenna can be modelled as a vertical current sheet inside the substrate as shown in Fig. 2.2. The radiation characteristics are calculated of such a magnetic current sheet are derived in this section.

2.2.1 Formulation of the Problem :

A sheet current can be treated as a superposition of line current sources placed adjacent to each other.

For a vertical current sheet the radiation field is therefore obtained by integrating the expression (12a) with respect to the variable 'a' varying from '0' to 'b'. The component H_{y1} of radiation field is given by the expression:

$$H_{y2}(r,\theta) = -\frac{\omega \varepsilon_o \varepsilon_r}{k_o u} \cdot \left(\frac{1}{2\pi k_o r}\right)^{1/2} e^{\,j(k_o r - \pi/4)} \; f_2(\theta) \qquad (14a)$$

$$\text{where} \quad f_2(\theta) = \frac{\cos\theta \, \sin(k_o u b)}{\varepsilon_r \cos\theta \; \cos(k_o u b) - j u \sin(k_o u b)} \qquad (14b)$$

The power radiated can be calculated from the expression (13a). Radiation resistance is calculated from the knowledge of radiated power and the strength of total magnetic current (in volts) across the sheet.

2.2.2 Numerical Results:

Radiation patterns for vertical sheet currents for an operating frequency of 3GHz are shown in Fig. 2.6. By comparing curves 2 and 3 it may be noted that an increase in ε_r or in height 'b' modifies the radiation pattern mainly in the end-fire direction.

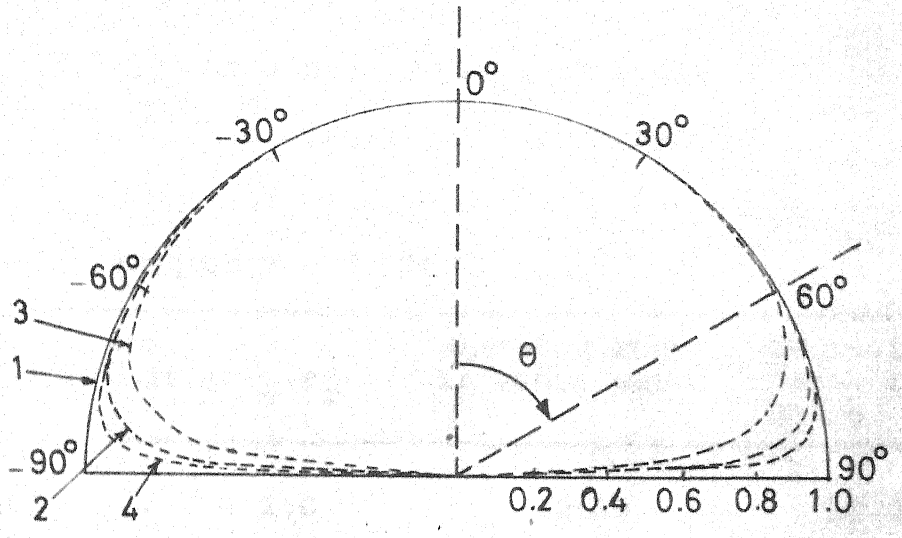

1. $\epsilon_r = 1$, b = 1/16", 1/8"
2. $\epsilon_r = 2.53$, b = 1/16"
3. $\epsilon_r = 2.53$, b = 1/8"
4. $\epsilon_r = 9.8$, b = 0.025"

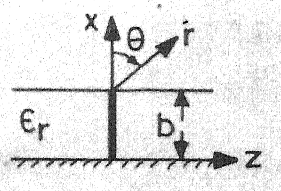

Fig. 2.6 Radiation pattern for vertical current sheets (Hy vs θ)

TABLE 2(b)

Radiated Power From Vertical Sheet

Type of source : Vertical Sheet

Strength of current = 1 Volt/m

Length of source = 1m

Frequency = 3 GHz

Height of the substrate b in metre	ε_r	Radiated Power in micro watts	Radiation Resistance in ohms/m metre
.00159	1.0	.2102	12.027
.00159	2.53	.20	12.640
.00328	1.0	.8895	12.094
.00328	2.53	.8156	13.190
.000635	1.0	.03357	12.011
.000635	9.8	.03273	12.319

Radiated power and the radiation resistance are tabulated in Table 2(b). The current dencity is in volts/m, and the power calculated is for an unit length (one metre) of source in y-direction.

2.3 A Horizontal Current Sheet on the Substrate:

In a microstrip antenna configuration (shown in Fig. 1.3) there is a horizontal component of fringing electric field. This component can be represented as a horizontal sheet of magnetic current on the top surface of the substrate. Radiation characteristics of such an aperture source are discussed in this section.

2.3.1 Formulation of the Problem:

Horizontal sheet of magnetic current on the substrate is treated as a superposition of continuously placed line currents on the substrate. The expression (12a) which gives radiation field for a line source inside the substrate is also valid when the line source lies on the substrate. The radiation field for two line sources positioned at (x=b, z=0) and x=b, z) is a vector sum of the fields for the two sources individually. It may be noted the two radi-

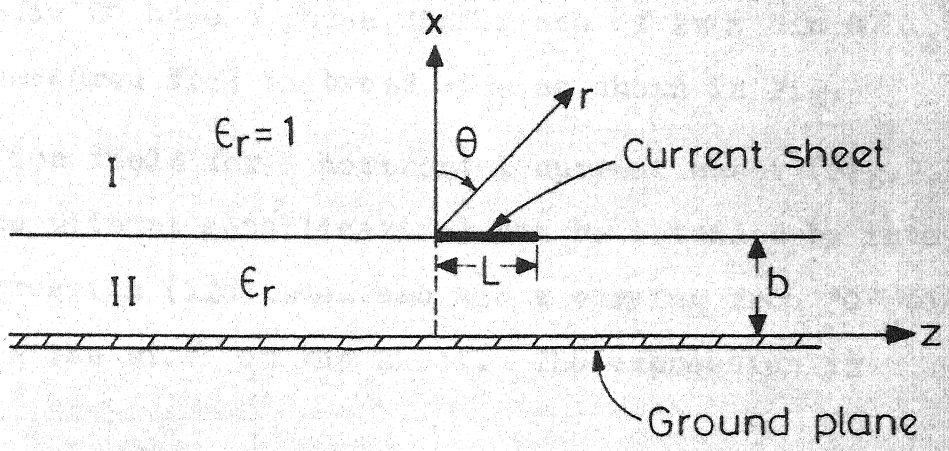

Fig. 2.3 An horizontal current sheet with one conducting plane.

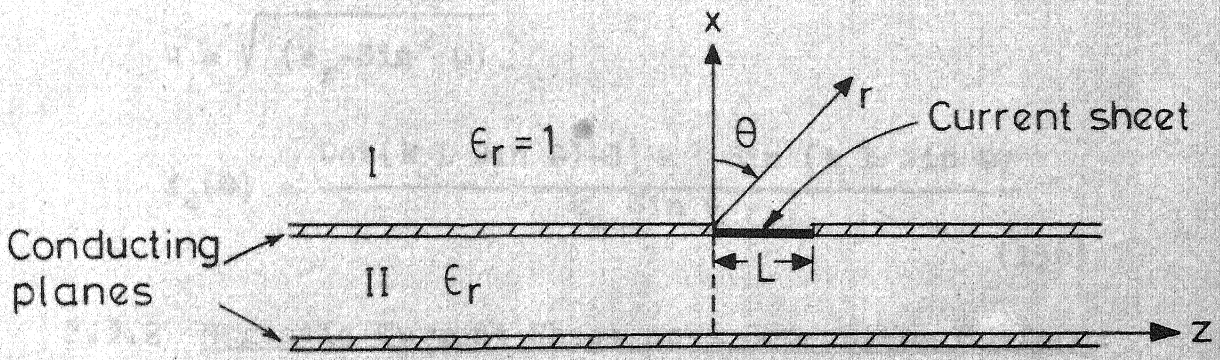

Fig. 2.4 An horizontal current sheet with two conducting planes.

ation fields have a phase difference of $2\pi(z \text{ Sin } \theta/\lambda_o)$; '$\theta$' being measured from the broad side as shown in Fig.

Radiation field for a horizontal current sheet (Fig.2.3) (top surface without metallization) can be obtained by integrating expression (12a) when a=b and z varying from '0' to 'L', L being the width of the sheet. The expression is

$$H_{y1}(r,\theta) = -\omega\varepsilon_o\varepsilon_r\left(\frac{1}{2\pi k_o r}\right)^{1/2} e^{\,j(k_o r-\pi/4)} \cdot f_3(\theta) \cdot f_4(\theta) \qquad (15a)$$

$$\text{where } f_3(\theta) = \frac{\text{Cos } \theta \;\; \text{Cos } (k_o ub)}{\varepsilon_r \text{ Cos } \theta \cdot \text{Cos}(k_o ub) - ju \text{ Sin}(k_o ub)} \qquad (15b)$$

$$u = \sqrt{(\varepsilon_r - \text{Sin}^2\,\theta)}$$

$$f_4(\theta) = \frac{j\{\text{Cos}(k_o L \text{ Sin } \theta) - 1\} + \text{Sin } (k_o L \text{ Sin } \theta)}{k_o \text{ Sin } \theta} \qquad (15c)$$

2.3.2 Magnetic Current Sheet on a Conducting Surface:

A horizontal magnetic current sheet on the substrate with top surface metallization [Fig. 2.4] is treated as a slot antenna of infinite length in y direction. In this configuration, the radiation field for a given current

distribution is independent of the substrate height and the value of ε_r. The magnetic current sheet can be expressed as a z directed E field distribution on the aperture. The maxwell's equation in transformed domain can be written as

$$\left(\frac{d^2}{dx^2} - h_o\right) \Psi_1 = 0. \tag{16a}$$

Solution for Ψ_1 in eqn (16a) can be written

$$\Psi_1 = M e^{-h_o x} \tag{16b}$$

with proper branch of h_o.

The boundary condition is that the E_z field is zero at every point of the top metallized plate except at the aperture. At aperture the field is $E_z = 1$.

In transformed domain the b.c. is

$$\frac{d\Psi_1}{dx}(b, \alpha) = \frac{\omega \varepsilon_o}{\alpha} [e^{jL} - 1] \tag{16c}$$

From 16a and 16 b one can write

$$H_{y1}(x,z) = \frac{1}{2\pi} \int_{-\infty}^{\infty} \frac{-\omega\varepsilon [e^{jL} - 1]\, e^{-h_o x}}{h_o e^{-h_o b}}\, d \tag{16d}$$

Employing steepest descent the for field may be written as

$$H_{y1}(r,\theta) = \omega\varepsilon \left(\frac{1}{2k_o \pi r}\right)^{\frac{1}{2}} e^{j(k_o r - \pi/4)} f_4(\theta) \tag{16e}$$

where $f_4(\theta)$ is given by (15c).

2.3.3 Numerical Results:

Radiation patterns for horizontal magnetic current sheet on a dielectric substrate (i) with top surface

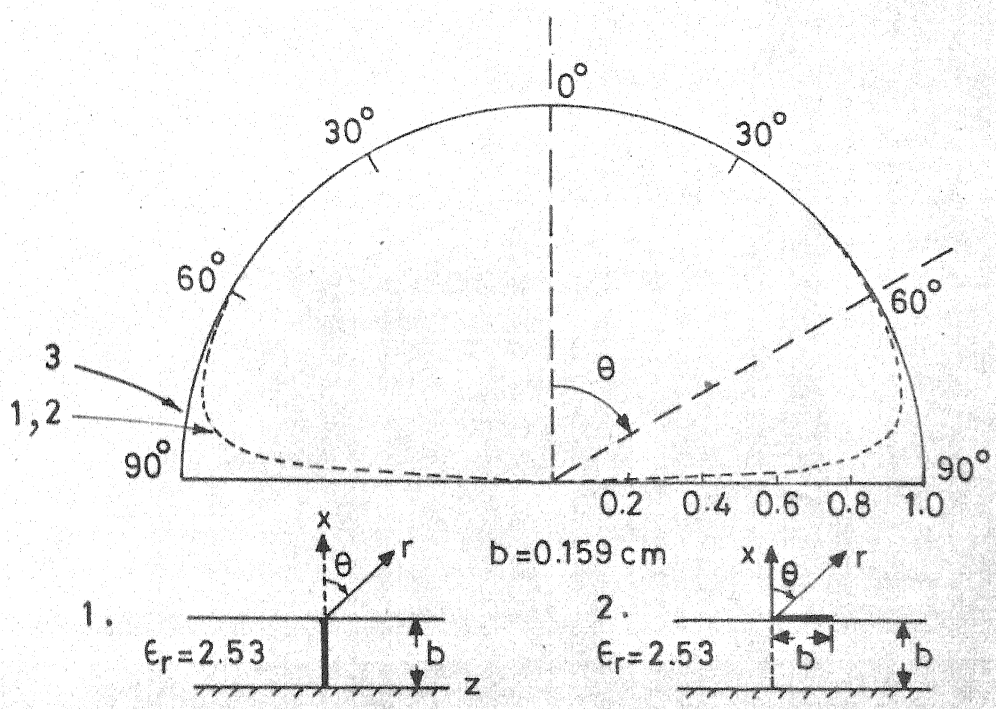

3. $\epsilon_r = 1.0$

Vertical or horizontal sheet

Fig. 2.8 Radiation pattern from vertical and a horizontal sheel ($|H_y|$ vs θ).

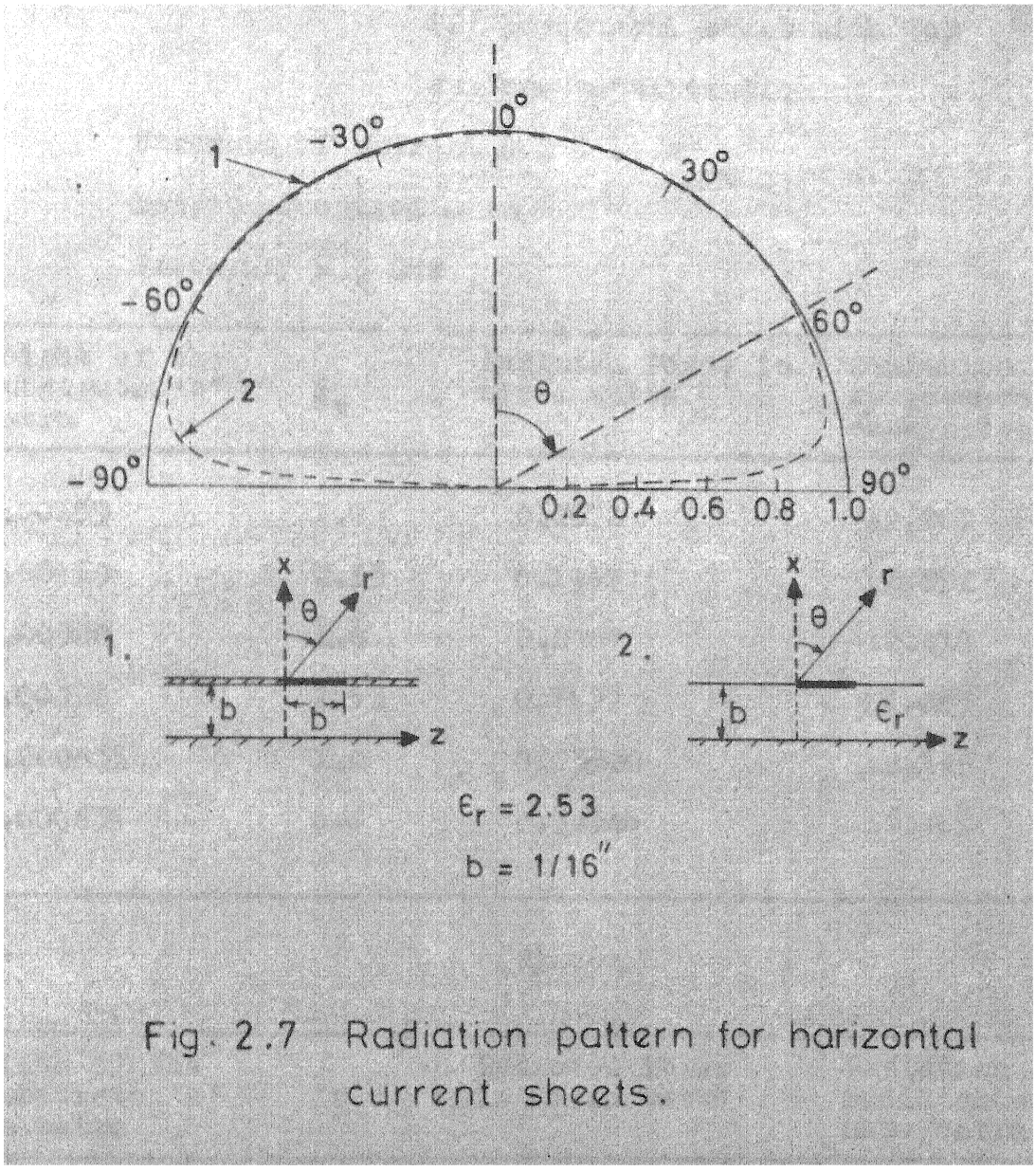

Fig. 2.7 Radiation pattern for horizontal current sheets.

Table 2(c)

Radiated Power from Horizontal Sheet

Type of source: (1) Horizontal Sheet (Top surface without metallization.

(2) Horizontal sheet with top surface metallization

Strength of current = 1 Volt/m

Length of source = 1m

Frequency = 3 GHz

(1)

Height of the substrate 'b' metre	ε_r	Radiated Power in micro watts	Radiation Resistance in ohms/metre
.00159	1.0	0.2072	12.201
.00159	2.53	0.1967	12.852
.00328	1.0	0.8667	12.413
.00328	2.53	0.7639	14.083
.000635	1.0	0.03320	12.145
.000635	o.8	0.32346	12.465

(2)

Width of the substrate 'b' in metre	ε_r	Radiated Power in micro watts	Radiation resistance in ohms/metre
0.00159	any value	0.2104	12.01
0.00328		0.8941	12.03

metalization (Fig.2.4) and (ii) without metalization (Fig. 2.3) are shown in Fig. 2.7. In the case (i), the radiation field in the broadside direction is about half that of without metalization (case ii). For the sheet with no metalization on the top surface (i.e. the case ii) the radiation pattern gets modified with increase in ε_r.

Radiated power for a current dencity of 1 volt/m for both the cases is tabulated in Table 2(c). The length of the source is 1 metre. Radiation resistance increases when either ε_r or height 'b' is increased.

2.4 Discussion:

Four types of magnetic current distributions studied in this chapter are:

(i) A magnetic current line source inside or on the dielectric substrate Fig. (2.1).

(ii) A vertical magnetic current sheet inside the dielectric substrate Fig. (2.2).

(iii) An horizontal magnetic current sheet on the substrate without metalization on top surface Fig. (2.3).

(iv) An horizontal magnetic current sheet on the substrate with metalization on top surface. Fig.(2.4).

Radiation patterns get modified by the presence of dielectric substrate in all the above cases other than the

the type (iv), when the relative permitivity of the substrate ε_r or height of the substrate 'b' are increased. For all these cases an increse in ε_r or increase in height 'b' reduces the field strength near the end-fire direction. For these three types of source the changes in radiation pattern are similar as shown in Figs. 2.5, 2.8.

Radiated power also decreases for an increase in ε_r or in height 'b' for the sources of the types (i), (ii) and (iii). A decrease in radiated power means an increase in radiation resistance. From the Tables 2(b) and 2(c) it is observed that radiation resistance for the horizontal current sheet of Fig. 2.3 is marginally greater than that of the vertical current sheet as shown in Fig.2.2.

Tables 2(a), 2(b) and 2(c) (for operating frequency of 3 GHz) show that with ε_r=1 the radiation resistance for all types of sources including the type (iv) have magnitudes which are in close agreement that obtained from the formula[17]

$$R = \frac{120\,\lambda_o}{1 - \frac{(k_o b)^2}{24}} \quad \text{ohm/m} \qquad (17)$$

where $\lambda_o \equiv$ free space wave length

$b \equiv$ height of the substrate.

The tables also show that for small heights with $\varepsilon_r \gg 1$ the radiation resistance calculated has values which closely agrees that given by expression (17).

CHAPTER 3

RADIATION FROM THE EDGE OF A SEMI-INFINITE SHEET ON A DIELECTRIC SUBSTRATE

Magnetic current source distributions discussed in in Chapter Two do not model the microstrip antennas accurately. Another configuration which can be used to investigate the radiation characteristics of these antennas is that of a semi-infinite conducting plate on the top surface of the dielectric substrate. This configuration (Fig. 3.1) may be analyzed by using Wiener-Hopf technique[10],[11].

3.1 Weiner-Hopf Analysis

3.1.1 Method of Analysis:

Consider a parallel plate wave-guide whose top plate is terminated abruptly as shown in Fig. 3.1. The yz coordinates are selected parallel to, and x-axis is chosen perpendicular to the conducting planes. The ground plate extends to whole of the yz plane and the top plate extends in y direction from $-\infty$ to ∞ and in z direction from $-\infty$ to 0. The wave-guide is filled by a dielectric substrate with a dielectric constant of ε_r. Let TEM incident field be travelling in the z direction as shown in Fig. 3.1. The incident field exists in the range $0 \leqslant x \leqslant b$ and $-\infty \leqslant z \leqslant \infty$

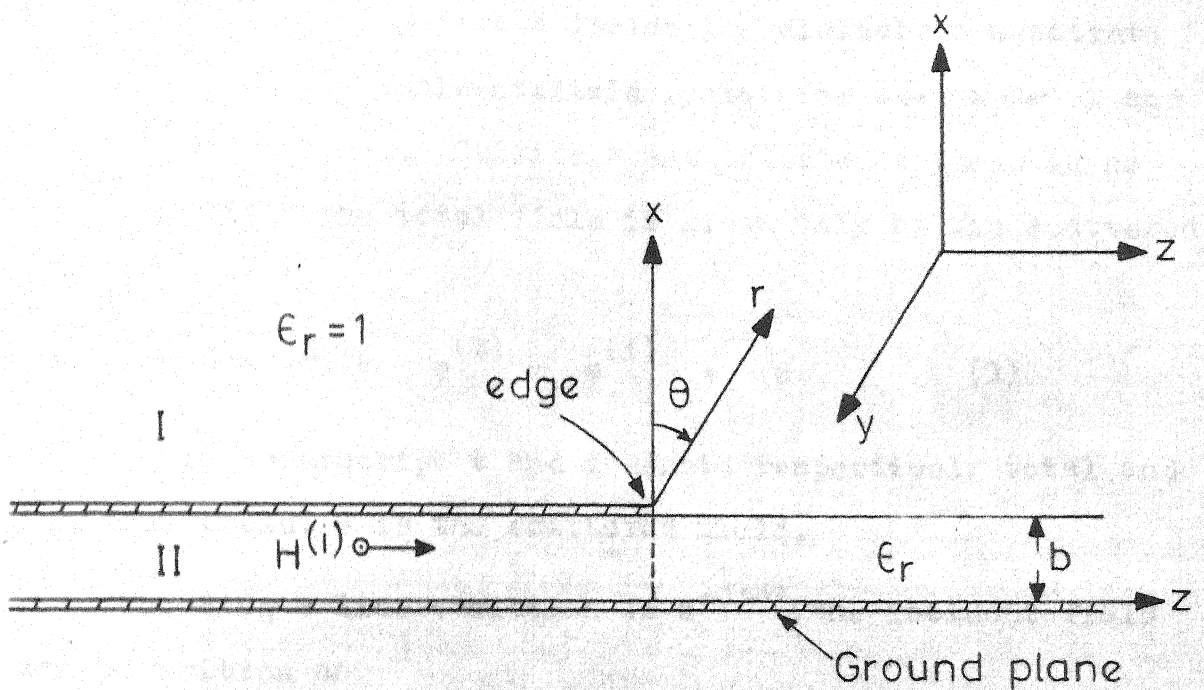

Fig . 3 .1 A truncated parallel plate waveguide .

and zero else where.

Due to the discontinuity in the top plate, there will be scattered fields both inside and outside the dielectric substrate. The total field inside the dielectric substrate is the sum of the incident field (exist for $-\infty < z < \infty$) and the scattered field. Outside the substrate as there is no incident field the total field is given only by the scattered field.

One can write $$\varphi^{(t)} = \varphi^{(i)} + \varphi \qquad (1)$$

where superscript t and i denote respectively total and incident field. φ is the scattered field.

Choosing a line variation of $e^{-j\omega t}$ the incident field can be written as

$$H_y^{(i)} = \varphi^{(i)} = e^{jk_d z} \qquad (2)$$

where $k_d = \sqrt{\varepsilon_r \ (\omega^2 \mu_o \varepsilon_o + j\omega \mu_o \sigma_2/\varepsilon_r)}$

$$= k_3 + jk_4$$

with $k_3 > 0$, $k_4 > 0$; for loss-less case $k_4 \longrightarrow 0^+$ and σ_2 is the conductivity of the substrate.

Electromagnetic fields are obtained by solving the wave equation for scalor potential φ.

There is no variation of fields in y direction; thus $\frac{\partial}{\partial y} = 0$ and φ satisfies the following wave equations.

$$(V_T^2 + k_d^2)\ \varphi = 0 \qquad 0 \leqslant x \leqslant b \qquad (3)$$

$$(V_T^2 + k^2)\ \varphi = 0 \qquad x \geqslant b \qquad (4)$$

where $V_T^2 = \frac{\partial^2}{\partial x^2} + \frac{\partial^2}{\partial z^2}$

$k = (\omega^2 \mu_o \varepsilon_o + j\omega\mu_o \sigma_1)^{1/2} = k_1 + jk_2$

with $k_1 > 0$ and $k_2 > 0$, for loss less case $k_2 \longrightarrow 0^+$.

It is assumed that $k_4 > k_2$.

Various components of the scattered electromagnetic field are obtained from the following relations. We have

$$H_y = \varphi \ ; \quad E_x = \frac{-j}{\omega k \varepsilon} \frac{\partial H_y}{\partial z} = \frac{-j}{\omega k \varepsilon} \frac{\partial \varphi}{\partial z} \qquad (5)$$

$$E_z = \frac{j}{\omega k \varepsilon} \frac{\partial \varphi}{\partial x}$$

Defining the propagation constant α as $\alpha = \sigma + j\tau$, the following Fourier Transforms with respect to z are introduced.

$$\psi(x, \alpha) = \psi_+(x, \alpha) + \psi_-(x, \alpha) = \frac{1}{\sqrt{2\pi}} \int_{-\infty}^{\infty} \varphi(x, z)\ e^{j\alpha z}\ dz \qquad (6a)$$

where $\Psi_+(x,\alpha) = \frac{1}{\sqrt{2\pi}} \int_0^\infty \varphi(x,z)\, e^{j\alpha z}\, dz$ (6b)

and $\Psi_-(x,\alpha) = \frac{1}{\sqrt{2\pi}} \int_{-\infty}^0 \varphi(x,z) e^{j\alpha z}\, dz$ (6c)

$$\Psi'(x,\alpha) = \Psi'_+(x,\alpha) + \Psi'_-(x,\alpha) = \frac{1}{\sqrt{2\pi}} \int_{-\infty}^{\infty} \frac{\partial}{\partial x} \varphi(x,z) e^{j\alpha z} dz \quad (7a)$$

where $\Psi'_+(x,\alpha) = \frac{1}{\sqrt{2\pi}} \int_0^\infty \frac{\partial}{\partial x} \varphi(x,z) e^{j\alpha z}\, dz$ (7b)

and $\Psi'_-(x,\alpha) = \frac{1}{\sqrt{2\pi}} \int_{-\infty}^0 \frac{\partial}{\partial x} \varphi(x,z) e^{j\alpha z}\, dz$ (7c)

The scattered field φ attenuates as rapidly as $\exp(-k_4|z|)$ as $|z| \to \infty$ inside the dielectric. Outside the dielectric it is radiated field and behaves asymtoically as

$$\varphi(x,z) \sim \frac{1}{r^{1/2}} \ominus e^{j(k_1+jk_2)r}$$

Where r is the distance from the edge to the observation point.

The scattered field φ attenuates as rapidly as $\exp(-k_2|z|)$ as $|z| \longrightarrow \infty$. Therefore $\Psi_+(x,\alpha)$ is analytic

in α plane at least for $\tau > -k_2$ and $\psi(x,\alpha)$ is analytic at least for $\tau > k_2$. Hence $\psi(x,\alpha)$ is analytic at least in the strip $-k_2 < \tau < k_2$ [10],[1].

Equations (3) and (4) are solved by employing Fourier transform technique. The boundary conditions are: i) continuity of tangential component of total electric and magnetic fields across the air-dielectric interface and ii) zero electric field at both the conducting planes. The tangential component of incident electric field is zero at x=0 and x=b. Thus the tangential scattered electric field is also continous across the interface. It may be recalled that incident fields exist only in the dielectric region $0 \leqslant x \leqslant b$.

Taking Fourier transforms of equation (3) and (4), one gets

$$\frac{d^2\psi(x,\alpha)}{dx^2} - \gamma_1^2\psi(x,\alpha) = 0 \qquad 0 \leqslant x \leqslant b \qquad (8a)$$

$$\frac{d^2\psi(x,\alpha)}{dx^2} - \gamma^2\psi(x,\alpha) = 0 \qquad x \geqslant b \qquad (8b)$$

where $\gamma_1^2 = \alpha^2 - k_d^2$ (9a)

$$\gamma^2 = \alpha^2 - k^2 \qquad (9b)$$

Following are the general solutions of equation (8a) and (8b).

$$\Psi'(x,\alpha) = A_1(\alpha)\, e^{\gamma_1 x} + A_2(\alpha)\, e^{-\gamma_1 x} \qquad 0 \leq x \leq b \qquad (10a)$$

$$\Psi(x,\alpha) = B_1(\alpha)\, e^{\gamma x} + B_2(\alpha)\, e^{-\gamma x} \qquad x \geq b \qquad (10b)$$

The sign of the root of γ (branch of γ) chosen should be such that it leads to an outward attenuating wave. This requires that γ has positive real part when $-k_2 < \tau < k_2$.

The boundary conditions in transformed domain are given below

(a) Tangential component of electric field (total or scattered) is zero at the ground plane.

$E_z = 0$; at $x = 0$, $-\infty < z < \infty$

using eqn(s) and (7a) one gets

$$\Psi'(0, \alpha) = 0 \qquad (11a)$$

(b) Tangential component of scattered electric field is zero at the top conducting plate.

$E_z = 0$; at $x = b$, $z < 0$

Using eqn(5) and 7(c)

$$\Psi'_-(b^+,\alpha) = \Psi'_-(b^-,\alpha) = 0 \qquad (11b)$$

(c) Tangential component of scattered electric field is continous in the air-dielectric interface.

$$E_z \Big|_{b^+} = E_z \Big|_{b^-}, \quad \text{at} \quad x=b, \quad z > 0$$

using eqn(5) and 7(b),

$$\varepsilon_r \Psi'_+ (b^+,\alpha) = \Psi'_+ (b^-,\alpha) \qquad (11c)$$

(d) Tangential component of total magnetic field is continous at air-dielectric interface.

$$H_y^{(t)} \Big|_{x=b^-} = H_y^{(t)} \Big|_{x=b^+} ; \text{ at } x=b, \ z > 0$$

$$H_y(b^-,z) + H_y^{(i)}(b^-,z) = H_y(b^+,z)$$

From eqn(2),

$$H_y(b^+,z) - H_y(b^-,z) = e^{j k_d z}$$

Taking Fourier transform of above equation.

$$\Psi_+(b^+,\alpha) - \Psi_+(b^-,\alpha) = \frac{1}{\sqrt{2\pi}} \int_0^\infty e^{j(k_d+\alpha)z} \, dz$$

$$= \frac{j}{\sqrt{2\pi}(\alpha+k_d)} \qquad (11d)$$

(e) Besides the boundary conditions given above, the fields have to satisfy edge condition for an unique solution of the wave equations. Edge condition requires that the electrical and magnetic energy stored in any finite neighbourhood of an edge must be finite. It gives that none of field components of (E,H) should grow more rapidly than $e^{-1+\tau}$ with $\tau > 0$ and $r \longrightarrow 0$ where r is the radial distance from the edge [10] The variation of fields near the edge can be written as,

$$H_y \sim z^{1/2} \quad \text{when} \quad z \longrightarrow 0^-$$

$$E_z \sim z^{1/2} \quad \text{when} \quad z \longrightarrow 0^+$$

The above two equations give the following variations,

$$\Psi'_+(b,\alpha) \quad \alpha^{-3/2} \quad \text{when} \quad \alpha \longrightarrow \infty$$

$$\Psi_-(b,\alpha) \quad \alpha^{-3/2} \quad \text{when} \quad \alpha \longrightarrow \infty \qquad \text{(11e)}$$

Applying boundary condition given by (11a) to (10a) one gets.

$$A_1(\alpha) = A_2(\alpha).$$

Also, the proper branch of γ gives that B_1 in (10b) must be zero. Equations (10a) and (10b) are rewritten as

$$\Psi(x,\alpha) = A(\alpha)\ \text{Cosh}\ (\gamma_1 x) \qquad 0 \leqslant x \leqslant b \qquad \text{(12a)}$$

$$\Psi(x,\alpha) = B(\alpha)\ e^{-\gamma x} \qquad x \geqslant b \qquad \text{(12b)}$$

Equations (12a) and (12b) are written in the following form at x=b.

$$\Psi_+(b^-,\alpha) + \Psi_-(b^-,\alpha) = A(\alpha)\ \text{Cosh}\ (\gamma_1 b) \qquad (13a)$$

$$\Psi_+(b^+,\alpha) + \Psi_-(b^+,\alpha) = B(\alpha)\ e^{-\gamma b} \qquad (13b)$$

Taking derivative of (13a) and (13b) at x=b, one gets

$$\Psi'_+(b^-,\alpha) + \Psi'_-(b^-,\alpha) = \gamma_1 A\ \text{Sinh}\ (\gamma_1 b) \qquad (14a)$$

$$\Psi'_+(b^+,\alpha) + \Psi'_-(b^+,\alpha) = -\gamma B e^{-\gamma b} \qquad (14b)$$

Equations (11b) and (14b) give

$$\Psi'_+(b^-,\alpha) = \gamma_1 A\ \text{Sinh}\ (\gamma_1 b) \qquad (15a)$$

$$\Psi'_+(b^+,\alpha) = -\gamma B(\alpha) e^{-\gamma b} \qquad (15b)$$

From (11c), (15a) and (15b) the following relation is obtained

$$-\varepsilon_r \gamma\ B(\alpha) e^{-\gamma b} = \gamma_1 A(\alpha)\ \text{Sinh}\ (\gamma_1 b) \qquad (16)$$

Substracting (13a) from (13b) gives,

$$\Psi_+(b^+,\alpha) - \Psi_+(b^-,\alpha) + \Psi_-(b^+,\alpha) - \Psi_-(b^-,\alpha)$$

$$= B(\alpha)e^{-\gamma b} - A(\alpha)\ \text{Cosh}\ (\gamma_1 b) \qquad (17)$$

The following relation is defined.

$$\Psi_{-}(b^{+},\alpha) - \Psi_{-}(b^{-},\alpha) = J_{-}(\alpha) \qquad (18)$$

Using boundary condition given by (11d) in (17) and (18) one gets,

$$\frac{j}{\sqrt{2\pi}\,(\alpha+k_d)} + J_{-}(\alpha) = B(\alpha)\, e^{-\gamma b} - A(\alpha)\, \mathrm{Cosh}\,(\gamma_1 b) \qquad (19)$$

In equation (19), $A(\alpha)$ and $B(\alpha)$ are substituted from eqn. (15a) and (15b). The substitution gives the following relation.

$$\frac{j}{\sqrt{2\pi}(\alpha+k_d)} + J_{-}(\alpha) = -\frac{\Psi'_{+}(b^{+},\alpha)}{\gamma} - \frac{\Psi_{+}(b^{-},\alpha)\ \mathrm{Cos}\ \gamma_1 b}{\gamma_1\ \mathrm{Sinh}\,(\gamma_1 b)} \qquad (20)$$

Using (11c) the above equation is rewritten as

$$\frac{j}{\sqrt{2\pi}(\alpha+k_d)} + J_{-}(\alpha) = -\Psi'_{+}(b^{-},\alpha)\ \frac{1}{\varepsilon_r \gamma} + \frac{\mathrm{Cosh}\,(\gamma_1 b)}{\gamma_1\ \mathrm{Sinh}\,(\gamma_1 b)}$$

$$= -\Psi'_{+}(b^{-},\alpha)\ \left(\frac{1}{\varepsilon_r b \gamma_1^{2}} \times \frac{1}{G(\alpha)}\right) \qquad (21a)$$

where $$G(\alpha) = \frac{\mathrm{Sinh}\,(\gamma_1 b)}{\gamma_1 b} \times \frac{\gamma}{\gamma_1\ \mathrm{Sinh}\,(\gamma_1 b) + \varepsilon_r \gamma\ \mathrm{Cosh}\,(\gamma_1 b)} \qquad (21b)$$

Let $G(\alpha)$ be factored as $G(\alpha) = G_+(\alpha)\ G_-(\alpha)$, where $G_+(\alpha)$ is analytic in the upper α plane defined by $\tau > -k_2$ and $G_-(\alpha)$ is analytic in the lower half α plane defined by $\tau < k_2$. Factorization of $G(\alpha)$ is described in Appendix (B).

Equation (21a) may be rewritten as

$$\frac{j(\alpha-k_d)G_-(\alpha)}{\sqrt{2\pi}\ (\alpha+k_d)} + J_-(\alpha)(\alpha-k_d)G_-(\alpha) = -\ \frac{\Psi'_+(b^-,\alpha)}{(\alpha+k_d)\varepsilon_r b\ G_+(\alpha)} \qquad (21e)$$

$$\text{Let}\quad S(\alpha) = \frac{j(\alpha-k_d)\ G_-(\alpha)}{\sqrt{2\pi}\ (\alpha+k_d)} = S_+(\alpha) + S_-(\alpha) \qquad (22a)$$

where $S_+(\alpha)$ is analytic in the upper half α plane defined by $\tau > -k_2$ and $S_-(\alpha)$ is analytic in the lower half α plane defined by $\tau < k_2$. Decomposition of $S(\alpha)$ into sum of $S_+(\alpha)$ and $S_-(\alpha)$ is described in Appendix (C).

$S_+(\alpha)$ and $S_-(\alpha)$ are given by the following expressions

$$S_+(\alpha) = \frac{-j\ G_-(-k_d)\ 2\ k_d}{\sqrt{2\pi}\ (\alpha+k_d)} \qquad (22b)$$

$$S_-(\alpha) = \frac{j}{\sqrt{2\pi}\ (\alpha+k_d)} \cdot [\ (\alpha-k_d)G_-(\alpha) + 2k_d\ G_-(-k_d)\ ] \qquad (22c)$$

Using (22), (21c) is written in the following form.

$$S_-(\alpha)+J_-(\alpha)(\alpha-k_d)G_-(\alpha)= -\frac{\Psi_+'(b-,\alpha)}{(\alpha+k_d)\varepsilon_r b\ G_+(\alpha)} - S_+(\alpha) \qquad (23)$$

Left hand side of above eqn is analytic in the lower half plane defined by $\tau < k_2$ and right hand side is analytic in the upper half α plane defined by $\tau > -k_2$. There are two unknowns (J_-, Ψ_+') in the eqn. From edge condition (eqn. 11e) and Liouvells thearem[11] both sides of eqn (21e) is zero. Thus from right hand side of eqn (23), one gets

$$\Psi_+'(b-,\alpha)= \frac{j\varepsilon_r b\ 2k_d\ G_+(k_d)}{\sqrt{2\pi}\ (\alpha+k_d)}\ (\alpha+k_d)\ G_+(\alpha)$$

$$= \frac{1}{\sqrt{2\pi}}\ j\ \varepsilon_r b\ 2\ k_d\ G_+(k_d)\ \ G_+(\alpha) \qquad (24)$$

From (15a), (15b), (11c) and (24), $A(\alpha)$ and $B(\alpha)$ are given by the following relations.

$$A(\alpha) = \frac{j\ \varepsilon_r b\ 2\ k_d\ \ G_+(k_d)}{\sqrt{2\pi}\ \ \gamma_1\ \text{Sin h}\ \gamma_1 b}\ G_+(\alpha) \qquad (25a)$$

$$B(\alpha) = -\frac{jb\ 2\ k_d\ \ \ G_+(k_d)}{\sqrt{2\pi}\ \gamma\ e^{-\gamma b}}\ G_+(\alpha) \qquad (25b)$$

3.1.2 Radiation Field

To find scattered field, (25a) and (25b) are substituted in (12a) and (12b), and then inverse Fourier transforms are taken.

In the region $x \geq b$ one gets

$$\varphi(x,z) = \frac{1}{\sqrt{2\pi}} \int_{-\infty}^{\infty} B(\alpha)\, e^{-\gamma x}\, e^{-j\alpha z}\, d\alpha \qquad (26a)$$

$$= -2jk_d b\, G_+(k_d) \frac{1}{2\pi} \int_{-\infty}^{\infty} \frac{G_+(\alpha)}{\gamma\, e^{-\gamma b}}\, e^{-(\gamma x + j\alpha z)}\, d\alpha \qquad (26b)$$

The above integration cannot be evaluated analytically. However, the far field may be obtained by using steepest descent method. Steepest descent method is described in Appendix (A). Employing this method the for field can be written as,

$$H_y = \varphi(r,\theta) = 2bk_d\, G(k_d) \left(\frac{1}{2\pi kr}\right)^{1/2} e^{j(kr-\pi/4)}\, G_+(-k\sin\theta) \qquad (26c)$$

$$kr \gg 1, \quad x > b$$

The cylindrical co-ordinate system used in the above equation is shown in Fig (3.1).

3.1.3 Reflection Coefficient:

Scattered field in region $x < b$ is obtained by taking inverse Fourier transform of equation (12a).

$$H_y = \varphi(x,z) = \frac{1}{\sqrt{2\pi}} \int_{-\infty}^{\infty} A(\alpha) \cosh(\gamma_1 x) e^{-j\alpha z} \, d\alpha \qquad (27a)$$

$$= -2\varepsilon_r b k_d G_+(k_d) \frac{1}{2\pi j} \int_{-\infty}^{\infty} \frac{G_+(\alpha) \cosh(\gamma_1 x)}{\gamma_1 \sinh(\gamma_1 b)} e^{-j\alpha z} d\alpha \qquad (28b)$$

Using $G_+(\alpha) = G(\alpha)/G_-(\alpha)$, eqn (28b) can be rewritten as

$$\varphi(x,z) = -\varepsilon_r k_d G_+(k_d) \frac{1}{\pi j} \int_{-\infty}^{\infty} \frac{\cosh(\gamma_1 x) u(\alpha) e^{-j\alpha z}}{(\alpha+k_d)(\alpha-k_d) G_-(\alpha)} d\alpha \qquad (28c)$$

where $$u(\alpha) = \frac{\gamma}{\gamma_1 \sinh(\gamma_1 b) + \varepsilon_r \gamma \cosh(\gamma_1 b)} \qquad (28d)$$

For $z < 0$, the contour in eqn (28c) may be closed in upper half $\alpha(\alpha = +jz)$ plane. The integrand has a pole at $\alpha = k_d$. This residue will give a field variation of $e^{-jk_d z}$ (Time variation is $e^{-j\omega t}$). For loss less case $k_4 \longrightarrow 0^+$ and this variation gives a propagating mode which travels

in -z direction. From eqn (28b) the other poles enclosed are at $\alpha=jy_n$, where

$$y_n = +\sqrt{(n\pi/b)^2 - k_d^2} \qquad , n = 1,2,3 \qquad (29a)$$

These poles give attenuated mode of y_n is real. Thus, there will be only one propagating mode as long as the following condition is satisfied.

$$\sqrt{\epsilon_r}\, k_o < \frac{\pi}{b}$$

or $$k_o b < \frac{\pi}{\sqrt{\epsilon_r}} \qquad (29b)$$

Assuming, the above condition being satisfied, the field inside the parallel plate and for long values of negative z has the variation of $e^{-jk_d z}$. This corresponds to the reflected wave. Denoting reflected magnetic field by $H_{yr}(x,z)$ one can write

$$H_{yr}(x,z) = - G_+(k_d) \frac{e^{-jk_d z}}{G_-(k_d)} \qquad (30a)$$

The above expression also can be written in the following

form (recalling that $G_-(k_d) = G(k_d)/G_+(k_d)$).

$$H_{yr}(x,z) = -\varepsilon_r \; G_+(k_d)^2 \; e^{-jk_d z} \qquad (30b)$$

Reflection coefficient is usually defined as the ratio of reflected field E^- to incident field E^+. Expression (30b) is the reflected H field for unit incident H field. Thus reflection coefficient R' ($R' = \frac{E^-}{E^+}$) can be written as

$$R' = \varepsilon_r \; G_+(k_d)^2 \; e^{-jk_d z} \qquad (30c)$$

It is noted that in expression (30c) the time variation is $e^{-j\omega t}$. One can write reflection coefficient in time variation $e^{j\omega t}$ by replacing all +j by -j in (30c). Thus eflection Coefficient R' is given by

$$R = \text{conjugate of } R' \qquad (\text{time } e^{j\omega t}) \qquad (30d)$$

3.1.4 Edge Impedance:

Considering the truncated parallel plate wave guide as a transmission line (Fig 3.2), the discontinuity effect due to truncation of the top plate can be equivalently expressed as a impedance Z_E connected at the plane of the edge (z=0). Impedance Z_E per unit width along x can be written as

$$Z_E = Z_0 \; \frac{1+R}{1-R} \qquad (31a)$$

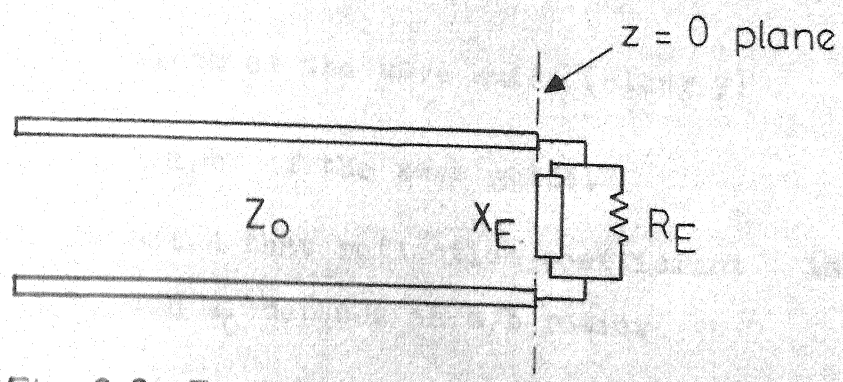

Fig. 3.2 Transmission line equivalent at the edge of the truncated parallel plate waveguide.

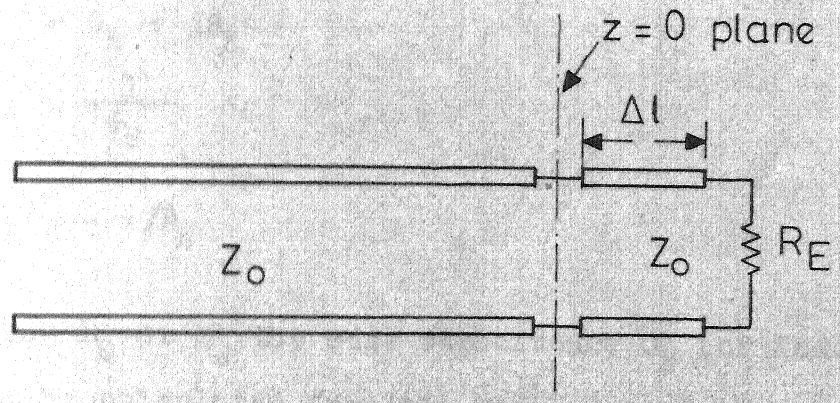

Fig. 3.3 Addition of a line section to represent edge capacitance.

where $Z_0 = \eta \frac{a}{b} = \sqrt{\mu_o/(\varepsilon_o \varepsilon_r)} \quad \frac{a}{b}$ (31b)

$a \equiv$ width of the wave guide (along y)

$b \equiv$ height of the wave guide.

It is to be noted that reflection coefficient is a function of $k_o b$, and Z_0 depends on a/b ratio.

The impedance Z_E can be represented as parallel combination of a resistance R_E and a reactance X_E. The parts R_E and X_E can be obtained using the following expressions

$$Y_E = 1/Z_E$$

$$Y_E = G_E + jB_E \qquad (32)$$

$$R_E = \frac{1}{G_E}$$

$$X_E = -1/B_E$$

From B_E or X_E the edge capacitance C_E (or inductance L_E) can be calculated from the knowledge of the operating frequency. The following two expressions give C_E or L_E depending upon the type of reactance.

$$C_E = B_E/\omega$$

$$L_E = X_E/\omega \qquad (33)$$

Equivalent Extension:

The reactance (usually capacitive) part of the edge impedance Z_E can be represented as a section of open circuited transmission line having same characteristic impedance as that of the parallel plate transmission line. In Fig 3.3 the edge capacitance C_E is shown as a section of the transmission line of length Δl.

3.2 Numerical Results:

Typical radiation patterns for radiation from one edge of a microstrip antenna modelled as a truncated waveguide (Fig. 3.1) are plotted in Figs 3.4 and 3.5 for some values of $k_o b$ and ε_r. From these patterns it is observed that an increase in ε_r reduces the field strength near end fire direction. In the other opposite direction ($\theta=-90^o$) the field strength increases. Another noteworthy feature is the fact that the radiation peak is not in broadside ($\theta=0$) but around $\theta=40^o$ towards the end-fire direction.

Variation of Reflection Coefficients with $k_o b$ is shown in Fig. 3.6. It is seen that reflection coefficient changes both in magnitude and phase with $k_o b$, higher the $k_o b$ value smaller is the reflection coefficient in magnitude.

From reflection coefficient 'R' and characteristic impedance of the line, the edge impedance is calculated. The impedance Z_E is found to be capacitive for the range of $k_o b$ (.1 to 1) considered. The edge resistance R_E and edge capacitance C_E are plotted in Figs 3.7 and 3.8 respectively.

Edge capacitance C_E can be expressed as a transmission line of length Δl. The normalized variation of extension $\Delta l/b$ with $k_o b$ is shown in Fig. 3.10.

In Fig. 3.9 a comparison is made among the values of edge or aperture resistance being calculated using the following methods (with operating frequency 3 GHz).

(1) by the formula [17].

$$R = \frac{120\,\lambda_o}{1 - \frac{(k_o b)^2}{24}}$$

(2) by the procedure described in Chapter Two (with $\varepsilon_r = 2.53$ for vertical sheet current)

(3) Weiner-Hopf technique (with $\varepsilon_r = 2.49$)

The curves are numbered accordingly. For lower value of $k_o b$, the results are similar but they do not agree for higher value of $k_o b$. Because of the nature of analysis procedure, the results based on Weiner-Hopf method should be considered most precise.

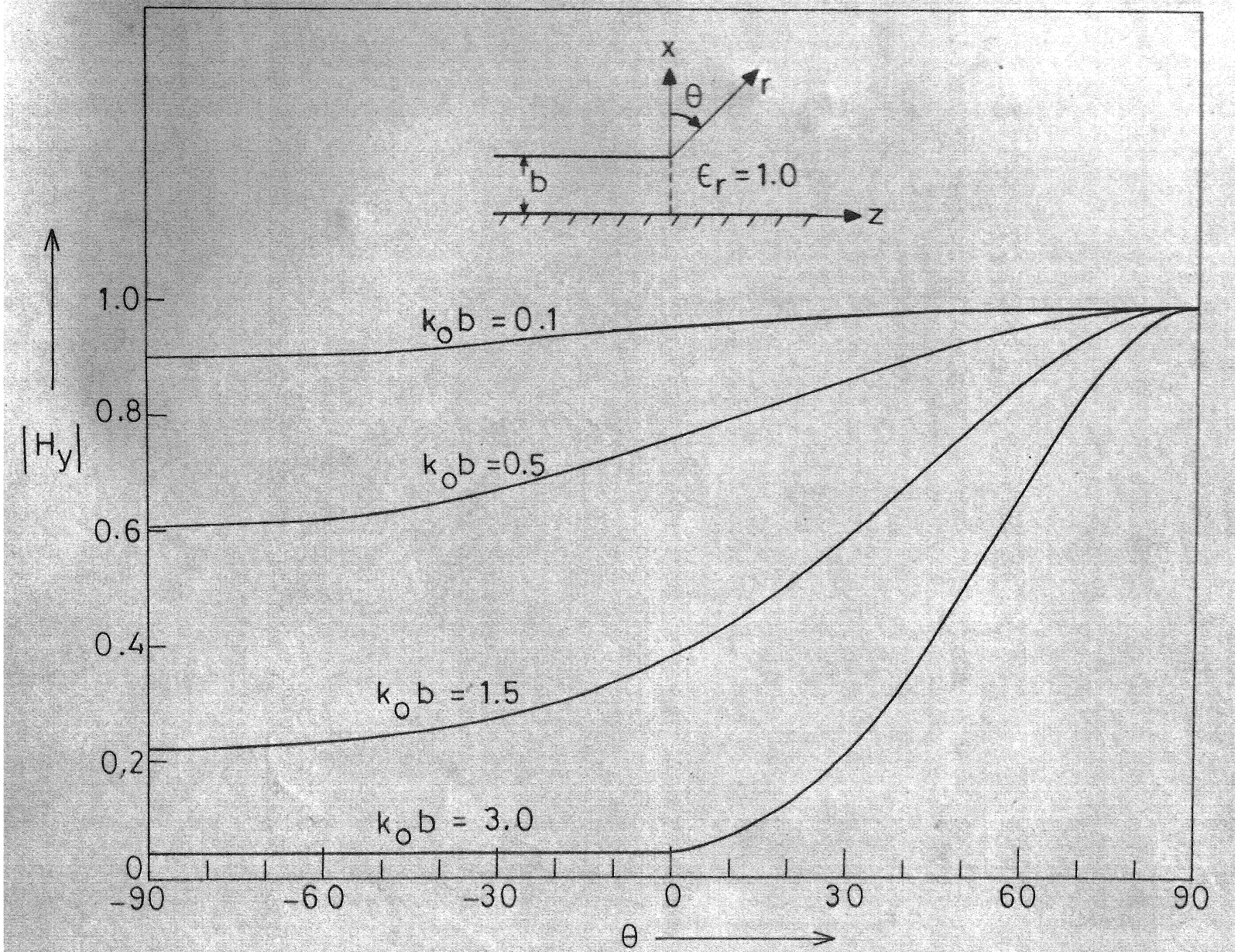

Fig. 3.4 Radiation pattern for the truncated waveguide $\epsilon_r = 1$.

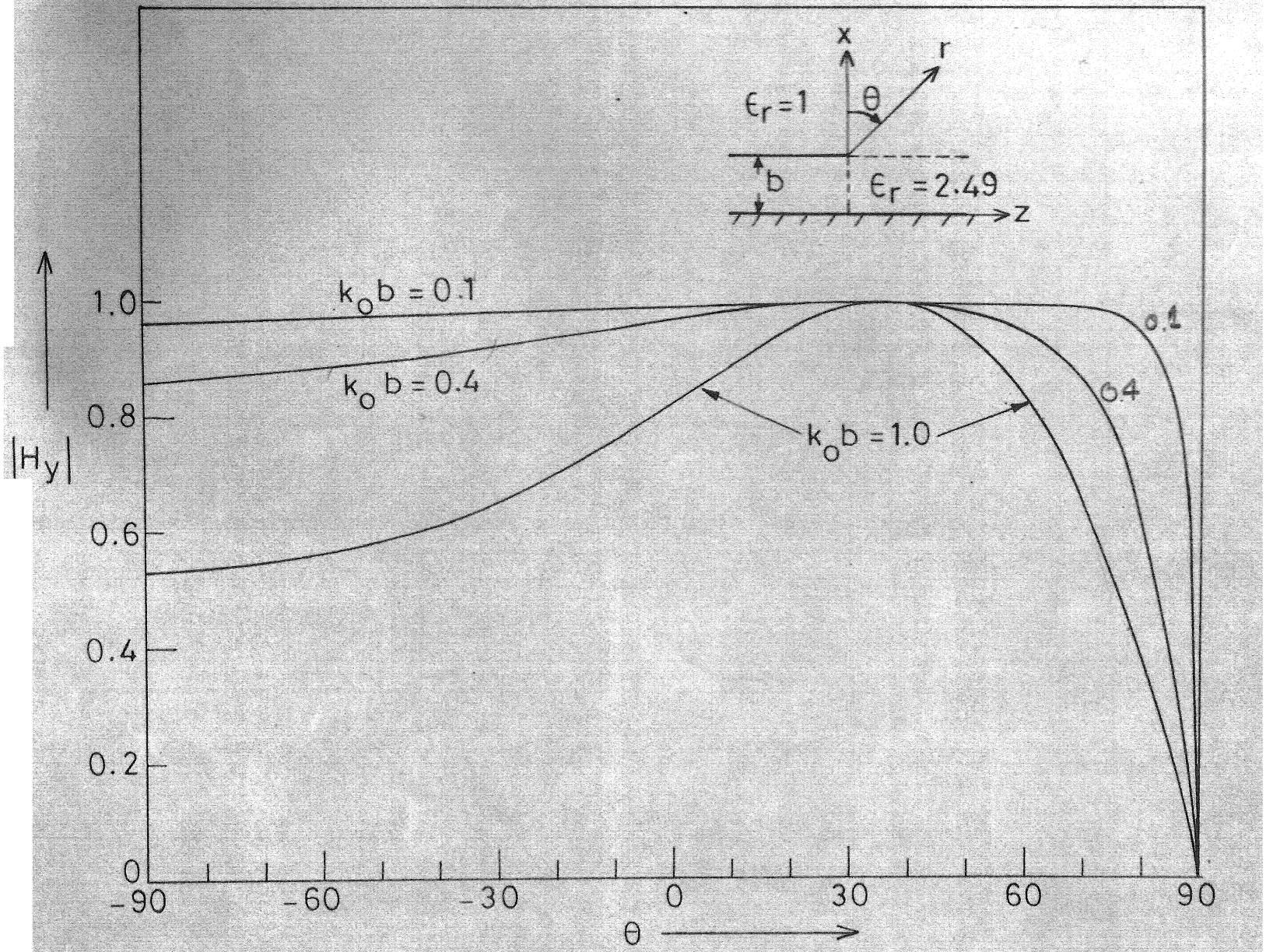

Fig. 3.5 Radiation pattern for the truncated waveguide with

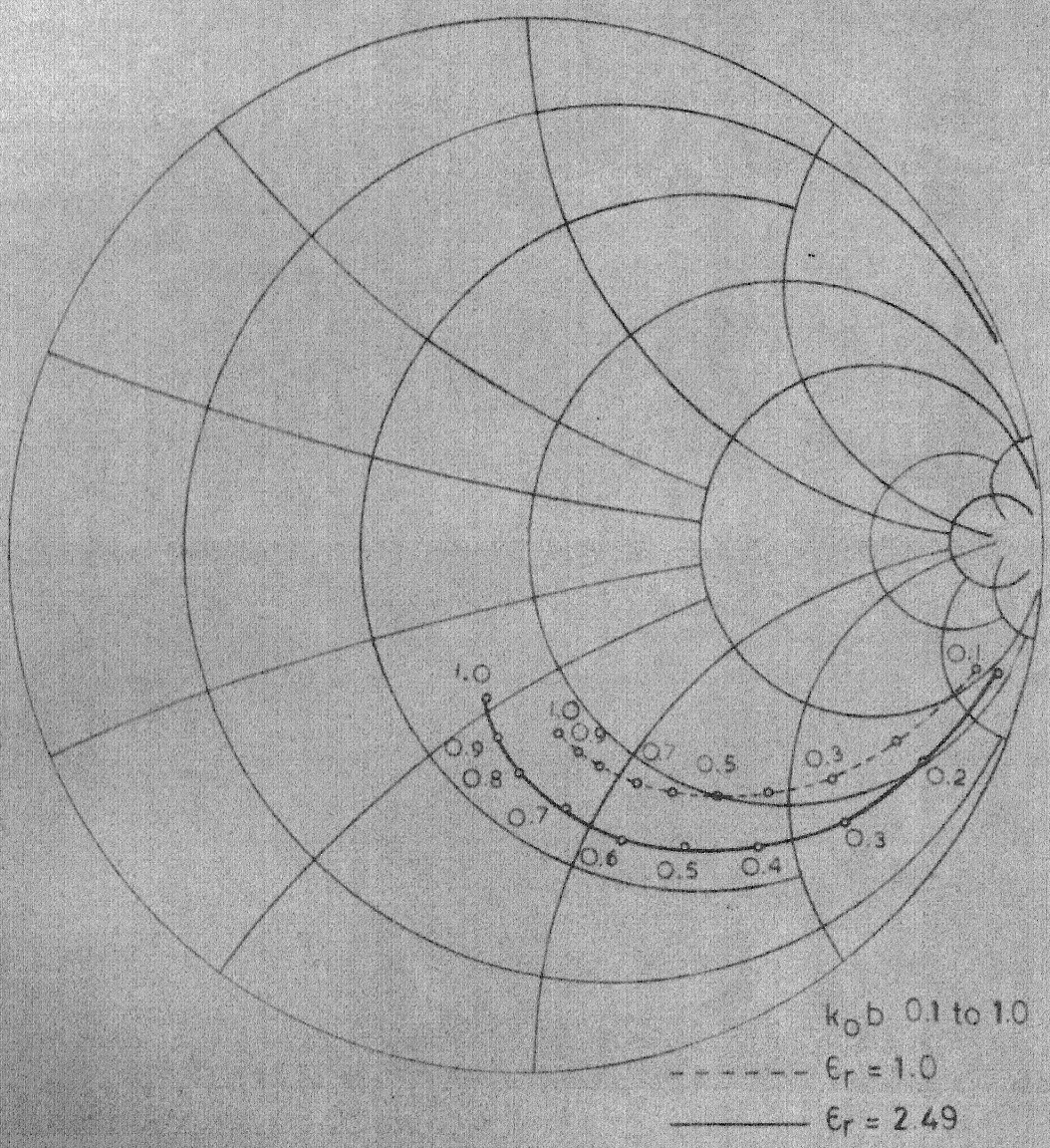

Fig. 3.6 Variation of reflection coefficient with $k_0 b$

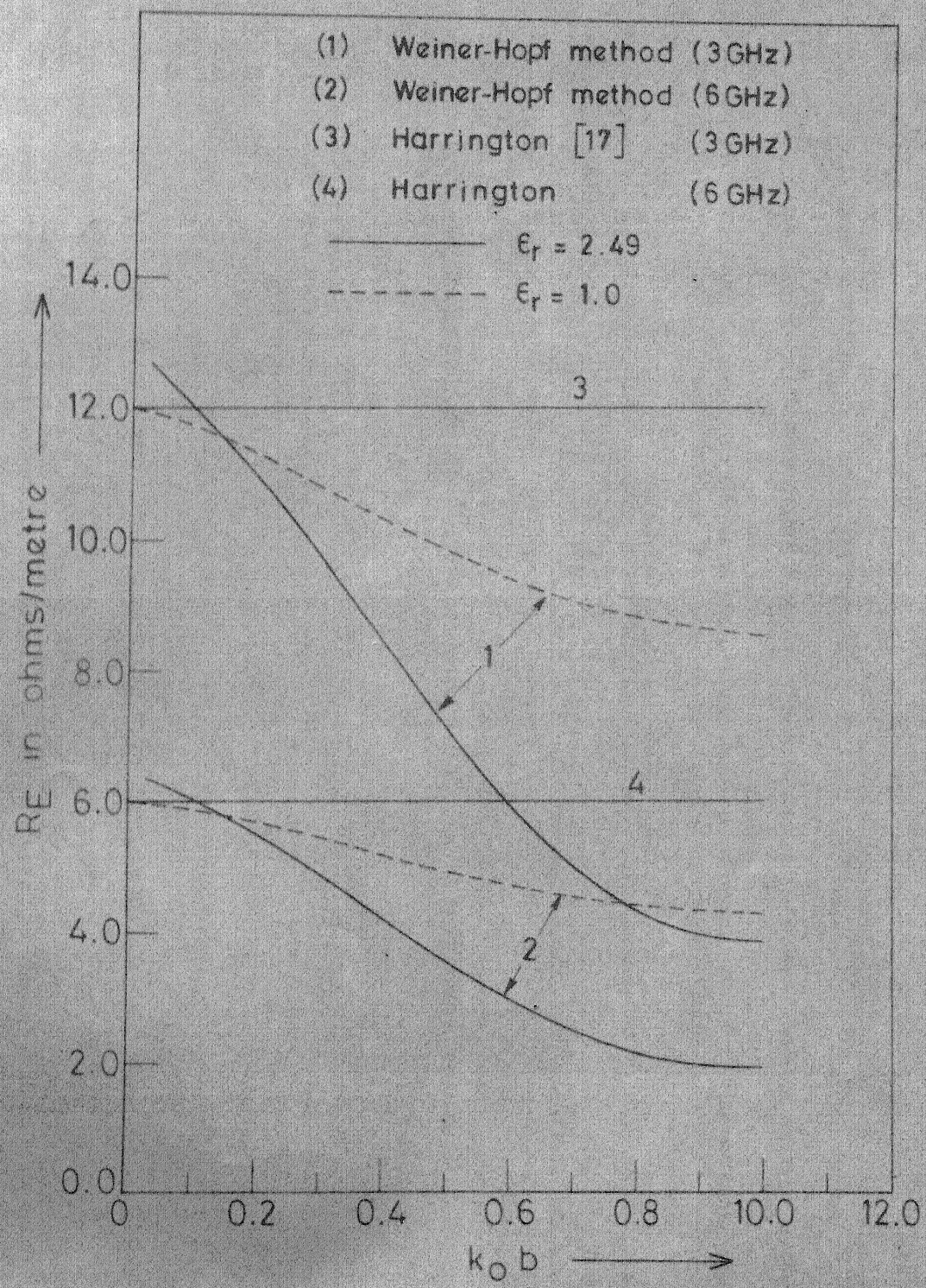

Fig. 3.7 Variation of edge resistance with $k_o b$.

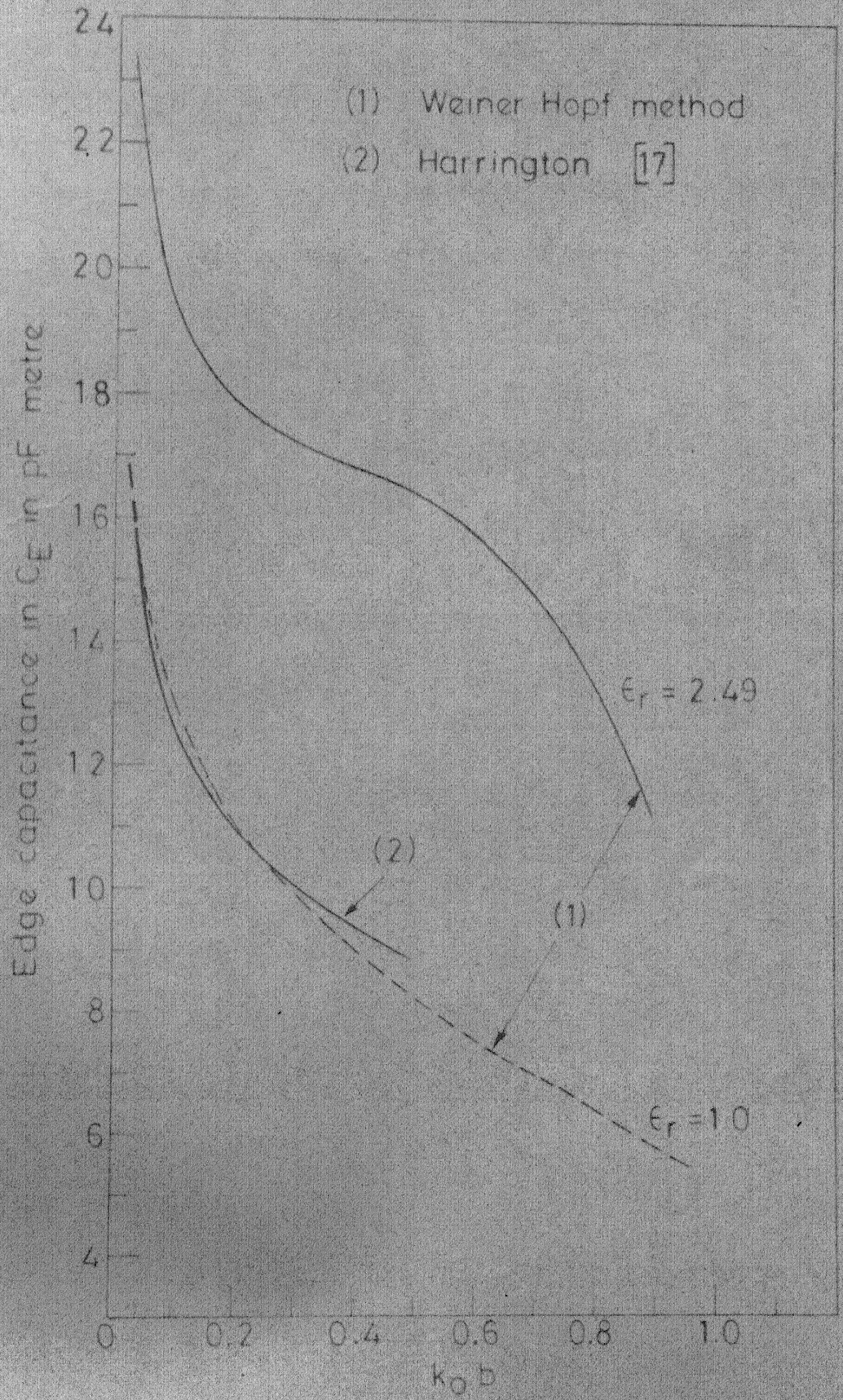

Fig. 3.8 Variation of edge capacitance with $k_0 b$

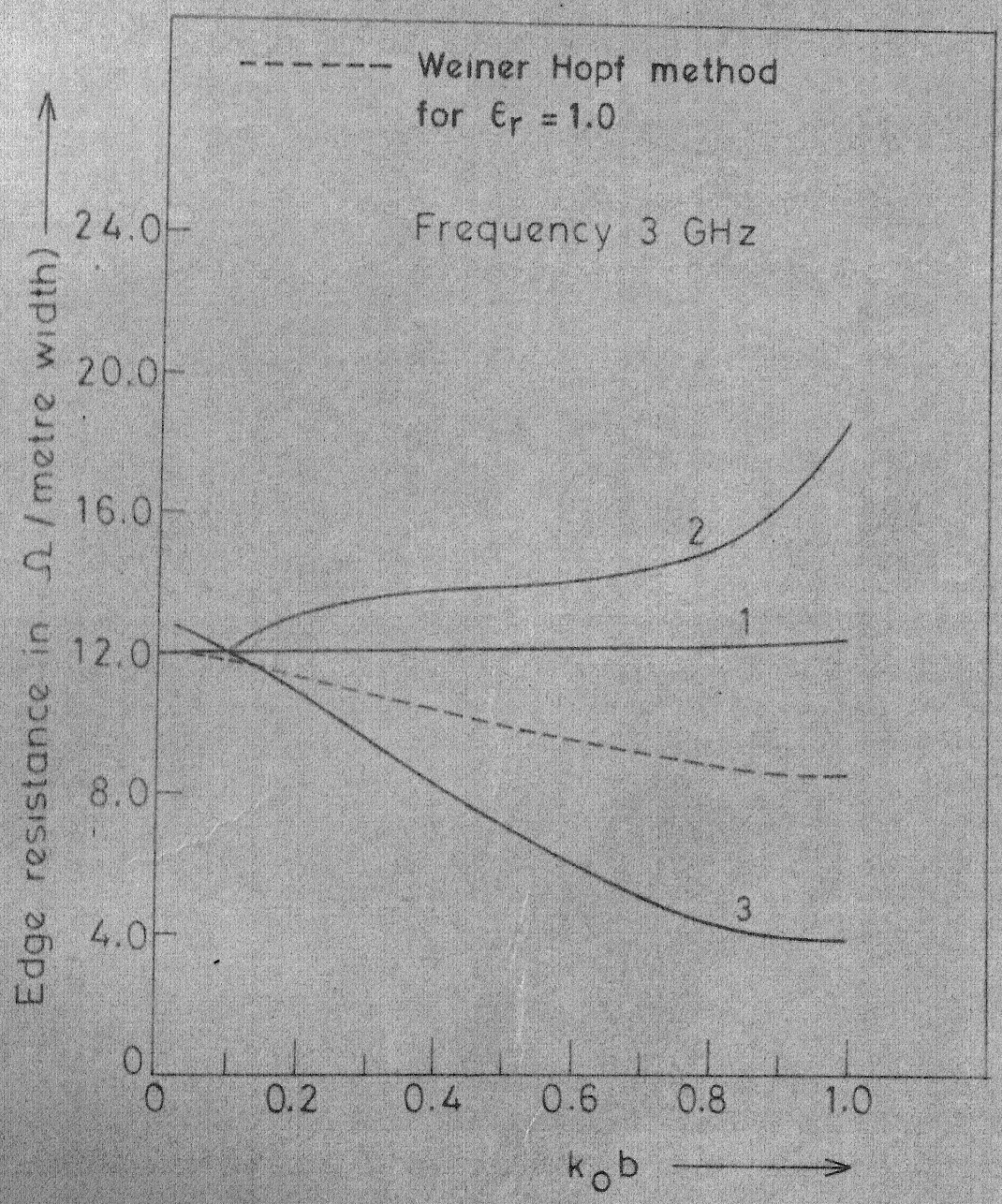

Fig. 3.9 Variation of radiation (or edge) resistance with $k_o b$.

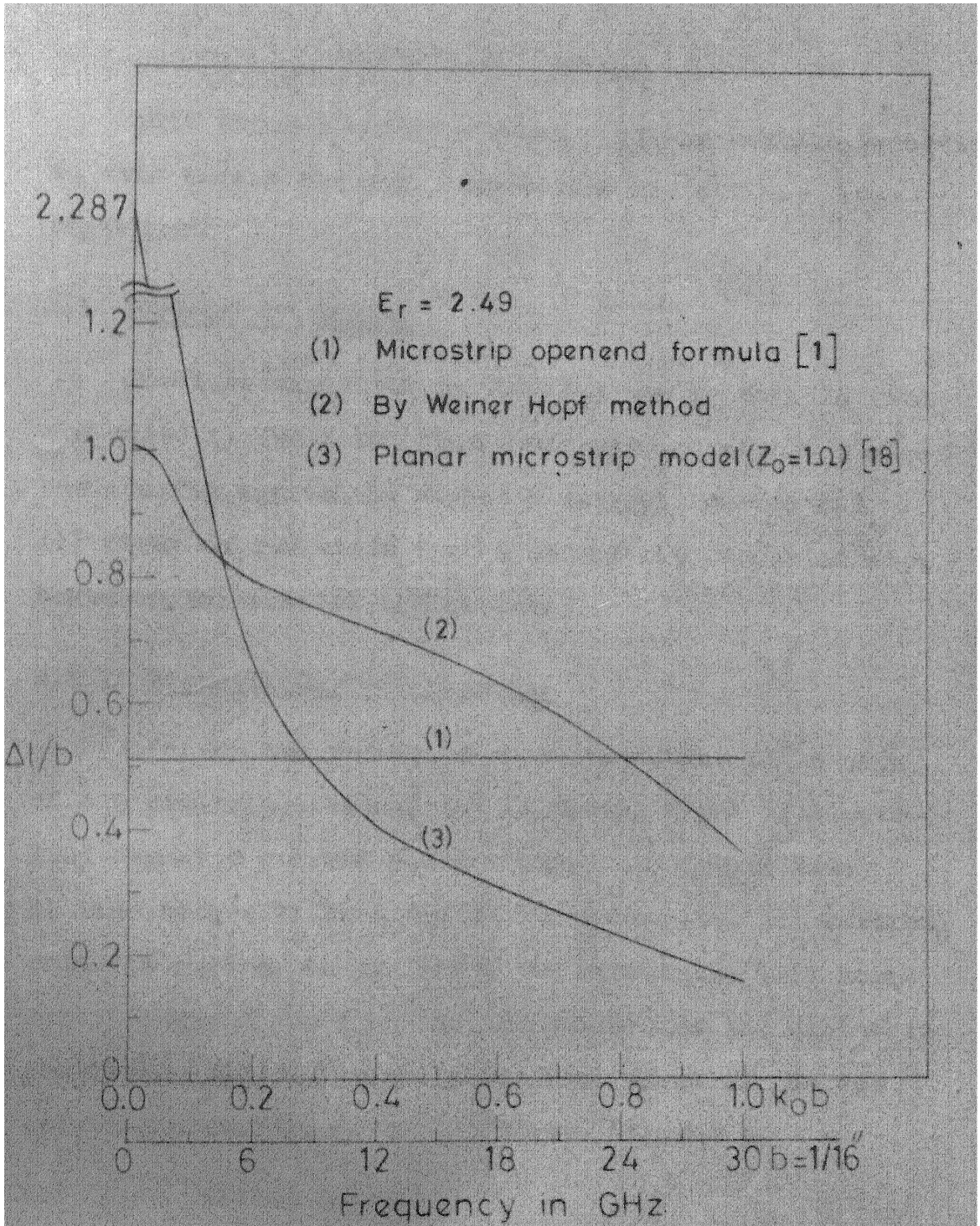

Fig. 3.10 Equivalent extention which represents edge capacitance.

CHAPTER 4

CONCLUDING REMARKS

This chpater contains summary of the results reported in this thesis and some suggestions for further investigations.

4.1 SUMMARY OF RESULTS:

The investigations carried out can be devided into two parts i) Radiation from a microstrip resonator edge by considering equivalent magnetic current sources and ii) Study of radiation from a microstrip resonator edge based on Weiner-Hopf techniques.

4.1.1 Magnetic Current Sources:

To study the radiation characteristics of an edge of a microstrip antenna, the following types of equivalent magnetic current sources have been considered: i) line source located inside the substrate, ii) vertical magnetic current sheet inside the substrate, iii) horizontal current sheet on the top surface of the dielectric substrate (Fig. 2.3), iv) horizontal sheet on the top metallized surface of the substrate (Fig2.4).

(i) Line Current Sources:

It is observed that for magnetic currents of equal strengths, a line current source located on the ground

plane radiates more power than that for the case when the line source is on the top surface of the substrate. The percentage difference in powers radiated in these two cases is about 2.2 percent for the case When ε_r=1, height of substrate 0.328 cm and the frequency is 3 GHz. This difference may be attributed to the fact that when the source is on the ground plane, the image with respect to the grounded plane produces a field in phase with the source field. When the air is replaced by a substrate with ε_r=2.53 the difference in the radiated powers is about 9 percent. The radiations patterns for these two positions of the source (for the thickness of the substrate considered i.e. b $< \frac{1}{8}$".) are very similar. For ε_r=1 the 3dβ points occur at angles $\pm 83^{o}$ from the broadside. Thus, the effect of the dielectric substrate is to reduce the total power radiated and to increase the directivity in broadside direction.

ii) Sheet Current Sources:

Comparing a horizontal sheet of magnetic current on the top surface of the substrate with a sheet placed vertically inside the substrate, it is observed that more power is radiated in the latter case. The difference is about 2.5 percent(strengths being equal). For ε_r=2.53,

this difference increases to about 6.5 percent . This may be explained by considering the current sheet as combinations of contigously placed line sources. For a vertical sheet there are more number of line sources which are close to their images than in the case of a horizontal current sheet.

4.1.2 Weiner-Hopf Approach:

The following noteworthy points emerge from the method based on Weiner-Hopf technique.

The radiation pattern for small $k_o b$ is nearly flat from -90° to 90° from the broadside (for $\varepsilon_r = 1$ and $\varepsilon_r = 2.49$). For $\varepsilon_r = 2.49$ the peak occurs at an angle of around 40° from broadside. As $k_o b$ increases, the radiated power in the positive θ direction increases.

The edge resistance R_E has been defined as the resistance corresponding to radiated and surface wave power leaving the edge. This resistance decreases with an increase in frequency. The values of edge resistance computed here differ from the calculations based on modelling the radiating edge as slot aperture in a ground plane [17]. In this slot aperture model the

radiation pattern is symmetric with respect to the broadside plane. Employing Weiner-Hopf technique we note that the radiation pattern is not symmetric for higher values of $k_o b (k_o b > 0.5)$.

Fringing field at the edge can be expressed in terms of an extension of the physical periphery such that the parallel plate capacitance added is equal to the fringing field capacitance associated with the edge. This extension normalized with the thickness of the substrate has been computed and is found to decrease with increasing frequency. The computed results have been compared with the following two case: i) the values that obtained by using the formula i) $\frac{\Delta l}{b} = 0.412 \left(\frac{\varepsilon_r + 0.3}{\varepsilon_r - 0.258}\right)$ when width $w \gg 1$, and ii) extension associated with the edge capacitance of a wide microstrip line ($Z_o = 5\,\Omega$). The extension in a microstrip line also decreases with increasing frequency but they agree closely only when $k_o b$ is very small (less than 0.1).

4.2 Suggestions For Further Investigations:

In the equivalent magnetic current approach the surface wave excitation has not been considered. If

surface wave power is evaluated, the radiation efficiency can be computed. Resistance of a radiating edge can be obtained by combining the radiation resistance with a resistance which represents the surface wave power.

Edge resistance R_E computed by the method based on Weiner-Hopf technique can be separated into two parts one of which is associated with radiated power and the other on surface wave power. This can be accomplished if radiated or surface power is calculated.

The edge impedance calculated by Weiner-Hopf method may be incorporated in the analysis of microstrip antennas of various shapes.

APPENDIX A

STEEPEST DESCENT METHOD

This appendix describes steepest descent method which is a asymptotic integration technique for the type of integral given below.

$$H_y(x,z) = \frac{1}{2\pi} \int_{-\infty}^{\infty} D(\beta)\, e^{j\beta z}\, e^{-h_o x}\, d\beta \qquad (A1)$$

where $h_o^2 = \beta^2 - k_o^2$ (A2)

This expression is used in chapter 2, to evaluate magnetic field in the air region from the line current source. There is a similar expression also in Chapter 3.

Using the polar coordinates Fig

$x = r \cos\theta$, $z = r \sin\theta$ (A3)

One can write (A1) as

$$H_y(r,\theta) = \frac{1}{2\pi} \int_{-\infty}^{\infty} D(\beta) e^{r(j\beta \sin\theta - h_o \cos\theta)}\, d\beta \qquad (A4)$$

The function h_o in (A4) is a two valued function and has branch points at $\beta = \pm k_o$. The proper branch of h_o should be such that it satisfies radiation condition. Specifically it requires

$$\mathrm{Re}\, h_o \geq 0$$
$$\mathrm{Im}\, h_o \leq 0 \qquad (A5)$$

For analytic convenience it can be assumed that the medium is slightly lossy; that is k_o has a very small positive imaginary part. The branch cuts, shown in Fig A1 satisfies the condition given by (A5).

Let, the following transformation be introduced.

$$\beta = k_o \text{ Sin } \phi = k_o \text{ Sin } (\xi + j\eta) \qquad (A6)$$

and its inverse transformation

$$\phi = \text{Sin}^{-1}(\beta/k_o) \qquad (A7)$$

The inverse sin is a multiple valued function and thus to ensure one to one mapping from β to φ plane, the inverse transformation is explicity defined as

$$\phi = -j \ln\left(j \frac{\beta + h_o}{k_o}\right) \qquad (A8)$$

In (A8), the logarithmic function is to be intrepreted as principal value type with argument of the function lying between $-\pi$ to π.

Transformations given by (A8), represents a mapping of the complex β-plane into a connected strip of the complex φ-plane. Fig (A1) and (A2) show the mapping of the two sheeted Rieman plane in to φ-plane. The four quadrants of the top and the bottom sheets of the β plane map into the regions denoted by T_i(top) and β_i(bottom) where i=1,2,3,4.

The contour of integration path, which is along the real axis in β-plane is indicated by C_o in Fig A1. The following relation is satisfied for the entire path of C_o.

$$h_o = \sqrt{(k_o \text{ Sin } \phi)^2} = -jk_o \text{ Cos } \phi \qquad (A9)$$

Substituting (A9) in (A4) one gets.

$$H_y(r,\theta) = \frac{1}{2\pi}\int_{C_o} k_o \text{ Cos } \phi D(k_o \text{ Sin } \phi)\, e^{k_o r\, g(\phi)} \qquad (A10)$$

where $g(\phi) = j \text{ Cos } (\phi - \theta)$ (A11)

The steepest descent method can be applied to (A10). The idea is to deform the path C_o in (A10) into a new path C_s, so that the integration can be approximated by integrating over a small portion of C_s. The criteria on the selection of this new path are that Re $g(\phi)$ have its maximum value at some point φ_s and decrease rapidly from ϕ_s. The point φ_s is known as saddle point and is determined by the following equation.

$$\frac{d\, g(\phi)}{d\phi}\bigg|_{\phi=\phi_s} = 0 \qquad (A12)$$

The path of steepest descent passes through the saddle point and the equation of the path is given by the equation

$$\text{Cos } (\phi - \theta) \text{ Cosh } \eta = 1 \qquad (A13)$$

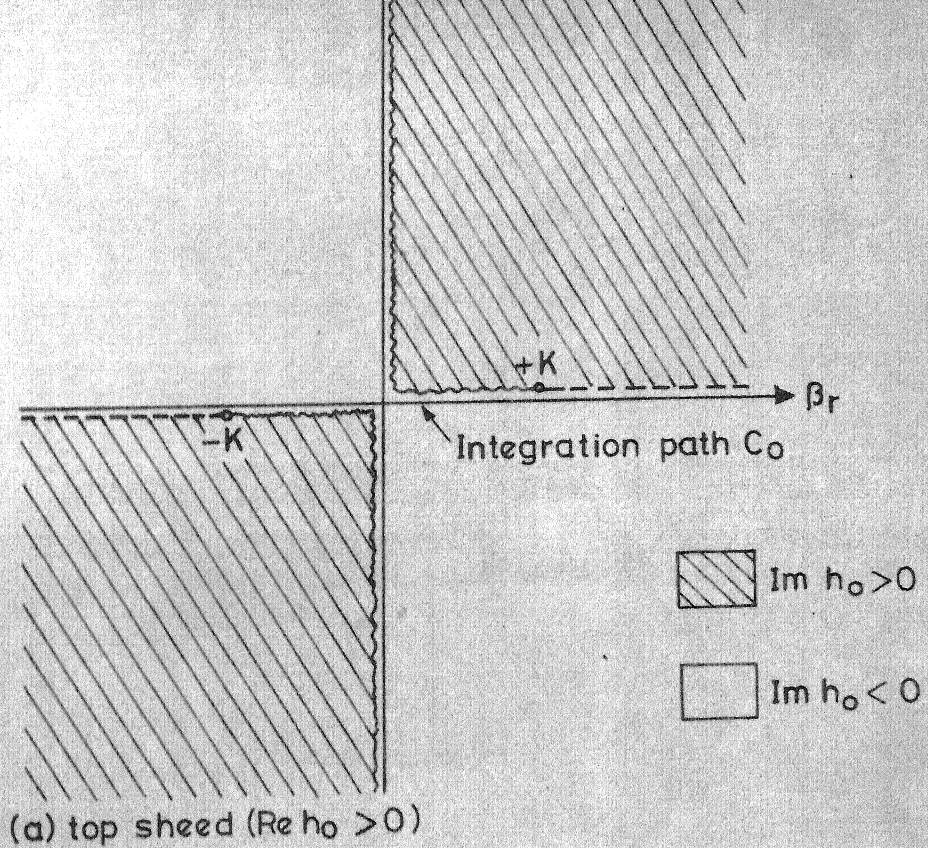

(a) top sheed (Re $h_o > 0$)

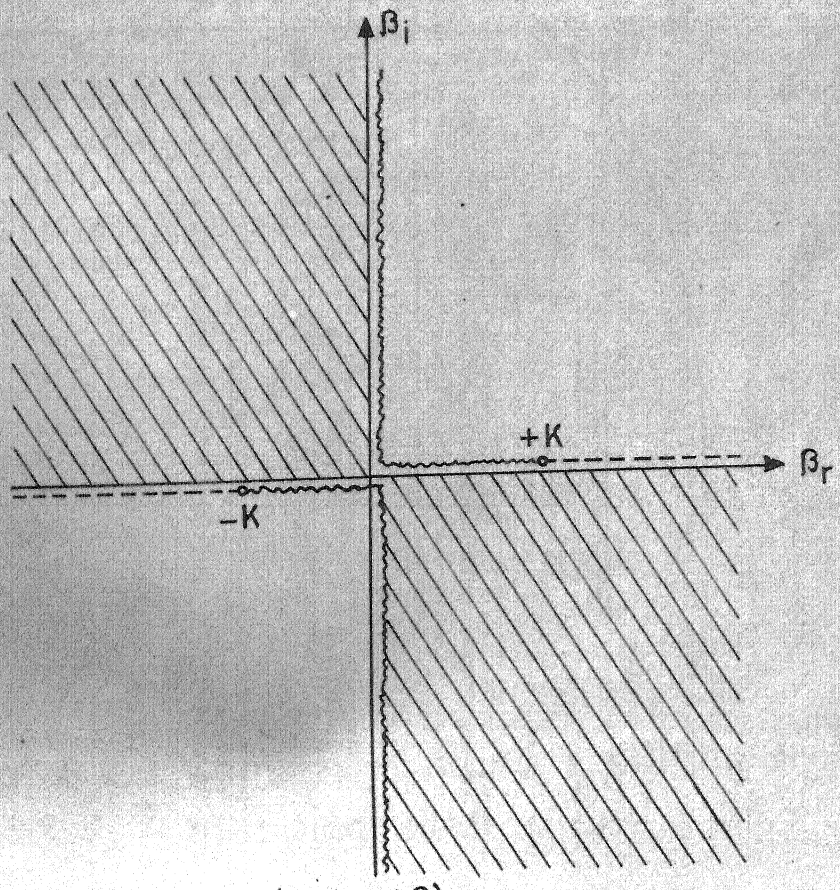

(b) bottom sheet (Re $h_o < 0$)

Fig. A1 Two sheets in the complex β-plane.

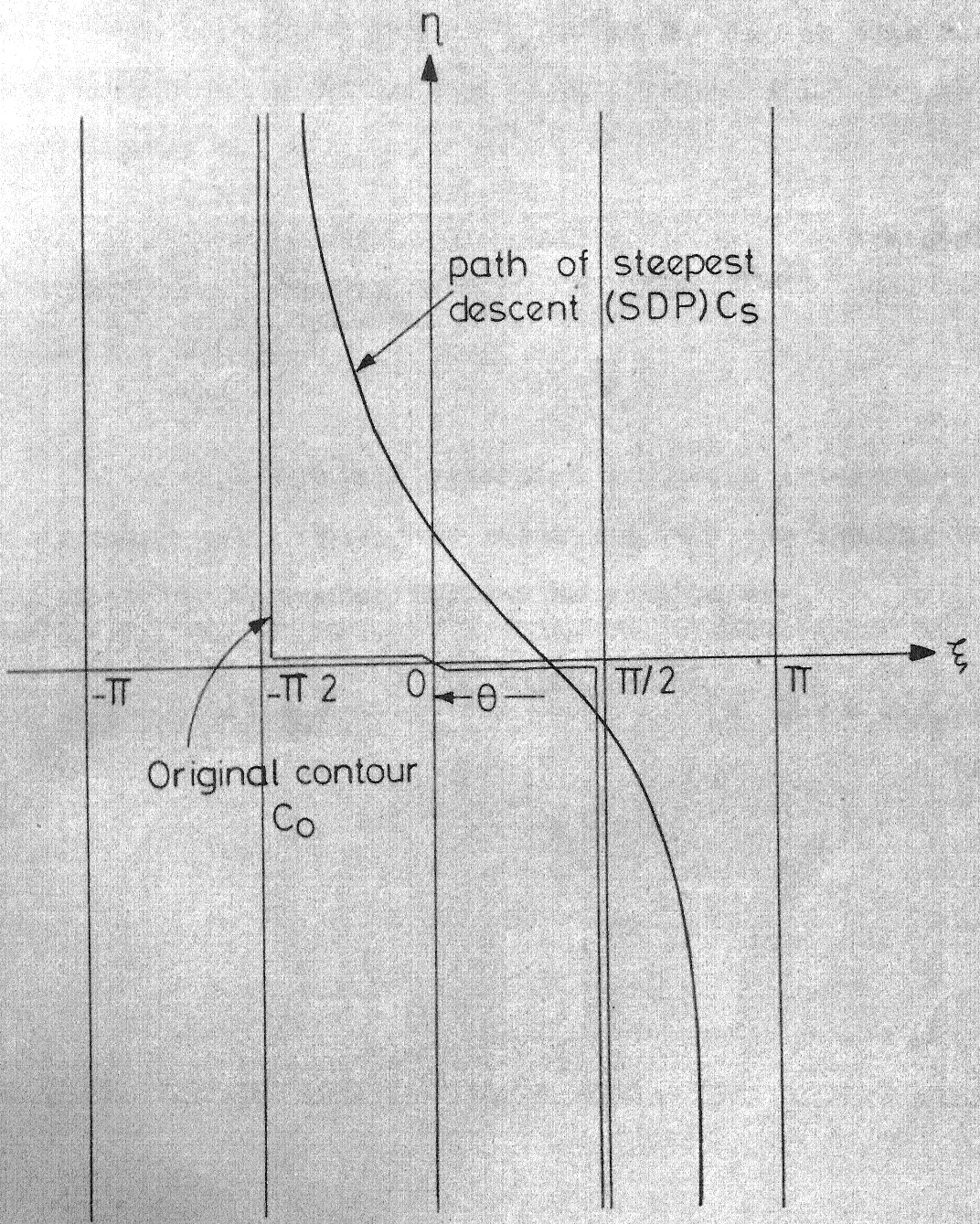

Fig. A 2 Complex ϕ-plane resulting from the mapping of β plane.

The main contribution of the integral given by A(10) comes from a small segment C_s around $\phi = \theta$. On this new path indicated by SDP in Fig A2 integration A(10) can be approximated as

$$H_y(r,\theta) \quad \frac{1}{2\pi} \int_{C_s} k_o \cos \phi \; D(k_o \sin \phi)\, e^{k_o r\, g(\phi)}\, d\phi \qquad (a14)$$

$$k_o r \gg 1$$

Using taylor series expansion the above integration can be expanded around $\phi=\theta$, and retaining only the leading term, the asymtotic approximation can be written as

$$H_y(r,\theta) \sim \left(\frac{1}{2\pi\, k_o r}\right)^{1/2} e^{j(k_o r - \pi/4)} [k_o \cos \theta \; D(k_o \sin \theta)] \qquad (A15)$$

$$k_o r \gg 1$$

APPENDIX B

FACTORIZATION OF $G(\alpha)$

This appendix describes the method for the factorization of the function $G(\alpha)$ appearing in Chapter 3. When factorization is carried out one can write $G(\alpha)$ as

$$G(\alpha) = G_+(\alpha) G_-(\alpha) \tag{B1}$$

where $G_+(\alpha)$ and $G_-(\alpha)$ are analytic and free of zeros in the upper and lower half α-planes defined by $\tau < k_2$ and $\tau > k_2$ respectively.

The function $G(\alpha)$ is given below

$$G(\alpha) = G^{(1)}(\alpha)\ G^{(2)}(\alpha) \tag{B2}$$

where $$G^{(1)}(\alpha) = \frac{\text{Sinh}\,(\gamma_1 b)}{\gamma_1 b} \tag{B3}$$

and $$G^{(2)}(\alpha) = \frac{\gamma}{\gamma_1 \text{ Sinh}(\gamma_1) + \varepsilon_r \gamma \text{ Cosh}\,(\gamma_1 b)} \tag{B4}$$

$G^{(1)}(\alpha)$ is an entire function and it can be expressed in the following infinite product form.

$$G^{(1)}(\alpha) = G^{(1)}(0) \prod_{n=1}^{\infty} \left(1 - \frac{\alpha}{jy_n}\right) e^{-j\alpha b/n\pi} \prod_{n=1}^{\infty} \left(1 + \frac{\alpha}{jy_n}\right) e^{j\alpha b/n\pi} \tag{B5}$$

where $\alpha = \pm jy_n$ are simple zeros of $G^{(1)}(\alpha)$ and Y_n is given by the relation

$$y_n = \sqrt{(n\pi/b)^2 - k_d^2} \qquad n=1,2,3 \qquad \text{(B6)}$$

From (B5) one can write,

$$G_+^{(1)}(\alpha) = \sqrt{G^{(1)}(0)} \prod_{n=1}^{\infty} (1+ \frac{\alpha}{jy_n}) e^{j\alpha b/n\pi} \qquad \text{(B7)}$$

$$G_-^{(1)}(\alpha) = \sqrt{G^{(1)}(0)} \prod_{n=1}^{\infty} (1- \frac{\alpha}{jy_n}) e^{-j\alpha b/n\pi} \qquad \text{(B8)}$$

with the asymptotic behaviour of $G_+(\alpha)$ given as [10]

$$G_-^{(1)}(\alpha) \sim A\alpha^{-1/2} \exp(jb\alpha/\pi) \exp[(-jb\alpha/\pi)\ 1-\ln(-jb\alpha/\pi)] \qquad \text{(B9)}$$

as $\alpha \longrightarrow \infty$

To factorize the function $G^{(2)}(\alpha)$, the formula derived by Bates and Mittra [13], is used. It is given as,

Let $G^{(2)}(\alpha)$ be an analytic function of α, and it satisfies the following conditions in the strip $|\tau| < \tau_+$.

(a) $G^{(2)}(\alpha)$ is analytic in the strip

(b) $G^{(2)}(\alpha)$ is non zero and even, that is $G^{(2)}(-\alpha) = G^{(2)}(+\alpha) \neq 0$.

(c) $G^{(2)}(\alpha)$ $B\alpha^{\nu} e^{-h|\alpha|}$ as σ , where ν and h real coefficients.

Then for α within the strip, one can write

$$G^{(2)}(\alpha) = G_+^{(2)}(\alpha)\, G_-^{(2)}(\alpha) \tag{B10}$$

where $G_+^{(2)}(\alpha)$ and $G_-^{(2)}(\alpha)$ are non zero and analytic in the upper ($\tau > \tau_-$) and lower ($\tau < \tau_+$) α-plane, respectively. The expressions for $G_+^{(2)}(\alpha)$ and $G_-^{(2)}(\alpha)$ are

$$G_+^{(2)}(\alpha) = G_-^{(2)}(\alpha) = \sqrt{G^{(2)}(0)}\,\left(1+\frac{\alpha}{k}\right)^{\nu_o/2} \prod_{m=1}^{M}\left(1+\frac{\alpha}{Z_m}\right) \times$$

$$\prod_{n=1}^{N}\left(1+\frac{\alpha}{Pn}\right) \exp\left[-\frac{jkh}{2} + \frac{jh\gamma}{\pi}\ln\left(\frac{\alpha-\gamma}{k}\right) + q(\alpha) + R_n(\alpha)\right] \tag{B11}$$

In the above expressions, the following terms should be interpreted as given below

$$q(\alpha) = \int_0^{\infty} k(w)\ln\left[1 + \frac{\alpha}{\sqrt{k^2 - w^2}}\right] dw \tag{B12}$$

where $k(w) = \frac{h}{\pi} - \frac{1}{2\pi j}\left[B(w) + B(-w)\right]$ (B13)

where $B(w) = \frac{d}{w}\ln\left(G\sqrt{k^2 - w^2}\right)$ (B14)

$$\nu_o = \operatorname{Lim}_{w \to 0}\; wB(w) \tag{B15}$$

$Z_m \equiv$ Simple zeros of $G^{(2)}(\alpha)$, where Im Z_m τ_+,

$m = 1, 2, 3 \ldots M$.

$P_n \equiv$ Simples poles of $G^{(2)}(\alpha)$, where Im $P_n < \tau_+$,
$n = 1,2,3 \ldots N$.

$R_n(\alpha) \equiv$ sum of the residue contributions from the poles of $B(w)$ on the positive real axis.

$\gamma = \sqrt{\alpha^2 - k^2}$ with proper branch

$k = k_1 + jk_2$, $k_1 > 0$ and $k_2 > \tau_+$

The asymptotic behaviour of $G^{(1)}(\alpha)$ is given as

$$G_+^{(2)}(\alpha) \sim \alpha^{\nu/2} \exp\left[-\frac{ib\alpha}{\pi} \ln\left(\frac{2\alpha}{\alpha}\right)\right] \qquad \text{(B16)}$$

The branch singularities of $G^{(2)}(\alpha)$ are at $\alpha = \pm k$.

From condition (c) the asymptotic behaviour of $G^{(2)}(\alpha)$ can be written as

$$G^{(2)}(\alpha) \sim e^{-\alpha b}, \qquad |\alpha| \longrightarrow \infty, \ |\tau| < \tau_- \qquad \text{(B17)}$$

Hence $\nu = 0$ and $h = b$. The function $G^{(2)}(\alpha)$ does not have any zeros, but has poles at $\alpha = \pm P_n$, $n = 1,2,3 \ldots N$.

The poles P_n are determined from the equation

$$\gamma_1 \operatorname{Sinh}(\gamma_1 b) + \varepsilon_r \gamma \operatorname{Cosh}(\gamma_1 b) \Big|_{\alpha = P_n} = 0 \qquad \text{(B18)}$$

Using (B14) the function $B(w)$ is computed and obtained as

$$B(w) = \frac{1}{w} + \frac{X + jY}{u} \qquad \text{(B19)}$$

where $X = w[b\,(w' - \varepsilon_r^2 w^2/w')\,\mathrm{Sin}\,w'b\,\mathrm{Cos}\,w'b + 1 + \mathrm{Cos}^2 w'b\,(\varepsilon_r^2 - 1)]$ (B20)

$$Y = \varepsilon_r \mathrm{Sin}\, w'b \mathrm{Cos}\, w'b \mathrm{Cos}\, w'b\,(w^2/w' - 1) + \varepsilon_r w^2 b \tag{B21}$$

$$u = (\varepsilon_r w \mathrm{Cos}\, w'b)^2 + (w' \mathrm{Sin}\, w'b)^2 \tag{B22}$$

with $w' = (w^2 + k_d^2 - k^2)^{1/2}$ (B23)

$B(w)$ does not have poles on the positive real axis, and thus $R_n(\alpha) = 0$.

Using (B15) and (B18) one gets

$$\nu_o = 1 \tag{B24}$$

Using (B13) and (B18) the function $k(w)$ is obtained as

$$K(w) = \frac{b}{\pi} - \frac{\varepsilon_r \mathrm{Sin}\, w'b \mathrm{Cos}\, w'b\,(\frac{w^2}{w'} - w') + \varepsilon_r w^2 b}{\pi\,(\varepsilon_r w \mathrm{Cos}\, w'b)^2 + (w' \mathrm{Sin}\, w'b)^2} \tag{B25}$$

Substituting all the above results in (B11) the function $G_+^{(2)}(\alpha)$ is computed to obtain

$$G_+^{(2)}(\alpha) = G_-^{(2)}(\alpha) = \sqrt{G^{(2)}(0)}\,(1+\frac{\alpha}{k})^{1/2} \prod_{n=1}^{N} (1 + \frac{\alpha}{Pn})^{-1}$$

$$\exp[-\frac{jkb}{2} + \frac{jb\gamma}{\pi} \ln(\frac{\alpha-\gamma}{k}) + q(\alpha)] \tag{B26}$$

where P_n is obtained from (B18), and $q(\alpha)$ is to be computed using (B25) and (B12).

The asymptotic behaviour of $G_+^{(2)}(\alpha)$ is obtained by using (B16). The result is, as $\alpha \longrightarrow \infty$ and $\tau > -\tau_\mp$

$$G_+^{(2)}(\alpha) \sim \exp\left[-\frac{jb\alpha}{\pi} \ln\left(\frac{2\alpha}{\alpha}\right)\right. \tag{B27}$$

The function $G+(\alpha)$ can be written as

$$G(\alpha) = e^{X(\alpha)}\, G_+^{(1)}(\alpha)\, G_\mp^{(2)}(\alpha) \tag{B28}$$

where $G_+^{(1)}(\alpha)$ and $G_\mp^{(2)}(\alpha)$ are given by (B7) and (B26) respectively. The term $e^{X(\alpha)}$ is necessary to have an unique factorization of $G(\alpha)$. The function $X(\alpha)$ is analytic in whole of the α-plane. To determine (α) one has to invoke edge condition. Edge condition imposes that $G_+(\alpha)$ and $G_-(\alpha)$ should have algebric behaviour for large α in the respective plane of regularity.

Using (B9) and (B27) asymtotic behaviour of $G+(\alpha)$ given by (B28), can be written as

$$G_+(\alpha) \sim A\alpha^{-1/2} \exp\left\{-\frac{jb\alpha}{\pi}\left[1-C+\ln\left(\frac{2\pi}{kb}\right)+ j\,\frac{\pi}{2}\right) + j\,\frac{\pi}{2}\right] + X(\alpha)\right\} \tag{B29}$$

From (B29) the function $X(\alpha)$ can be choosen to have

$$X(\alpha) = \frac{jb\alpha}{\pi}\left[1 - C + \ln\left(\frac{2\pi}{kb}\right) + j\,\frac{\pi}{2}\right] \tag{B30}$$

where $C = 57721$ is Euler's constant.

Finally, using (B28), (B7), (B26) and (B30) the function G+(α) is obtained as given below.

$$G-(\alpha) = \sqrt{f(0)}\ (1+\frac{\alpha}{k})^{1/2} \prod_{n=1}^{\infty}(1+\frac{\alpha}{jy_n})e^{j\alpha b/n\pi} \prod_{n=1}^{N}(1+\frac{\alpha}{n})^{-1}$$

$$\exp\left[-\frac{jk_b}{2} + \frac{jb\gamma}{\pi}\ln\left(\frac{\alpha-\gamma}{k}\right) + q(\alpha)\right]$$

$$\exp\left[\frac{jb\alpha}{\pi}\ 1-C+\ln\left(\frac{2\pi}{k_b}\right) + j\ \pi/2\right] \qquad \text{(B31)}$$

where $$f(0) = \frac{k\ \text{Sin}\ k_d b}{k_d b\ \varepsilon_r k\ \text{Cos}\ (k_d b) - jk_d\ \text{Sin}\ (k_d b)} \qquad \text{(B32)}$$

Appendix C

DECOMPOSITION OF FUNCTION S(α)

This appendix describes the method of decomposition of function $S(\alpha)$ into the form $S(\alpha)=S_+(\alpha)+S_-(\alpha)$ where $S_+(\alpha)$, $S_-(\alpha)$ are analytic in the upper and lower half α-plane defined by $\tau > -k_2$ and $\tau < k_2$ respectively.

The function $S(\alpha)$ (Chapter 3) is given by the expression,

$$S(\alpha) = \frac{j(\alpha - k_d)\, G_-(\alpha)}{\sqrt{2\pi}\,(\alpha + k_d)} \qquad (1c)$$

The function $G_-(\alpha)$ is analytic in the lower half α-plane and so only discrete pole at the lower by half α-plane is at $\alpha=-k_d$. Following the standard method [10], [11], one can write,

$$S_+(\alpha) = \frac{-j2k_d\, G_-(-k_d)}{\sqrt{2\pi}(\alpha + k_d)}$$

$$= \frac{j2\, k_d\, G_+(k_d)}{\sqrt{2\pi}\,(\alpha + k_d)}$$

and $S_-(\alpha) = S(\alpha) - S_+(\alpha)$

$$= \frac{j}{\sqrt{2\pi}\,(\alpha + k_d)}\left[(\alpha-k_d)\, G_-(\alpha) + 2k_d\, G_-(-k_d)\right]$$

REFERENCES

1. I.J. Bahl and P. Bhartia, Microstrip Antennas. Dedham, MA: Artech House, 1980.

2. J.R. James and H. Hall, 'Microstrip Antennas and Arrays Pt I - Fundamental Action and Limitations'. IEE Journal MOA Vol. 1, PP. 175-181, 1977.

3. YT.LO., D. Solomon and W.F. Richards 'Theory and Experiment on Microstrip Antennas', IEEE Trans. Antennas Propagat., Vol. AP-27, PP. 846-849, 1979.

4. K. R. Corver and E.L. Coffey, 'Theoritical investigation of the Microstrip Antenna'. Tech. Rept. PT-00929, Physical Science Laboratory New Mexico State University, Las Guces (New Mexico) Jan. 1979.

5. R.E. Munson, ' Conformal Microstrip Antennas and Microstrip phased Arrays', IEEE Trans. Antennas Propagat., Vol. AP-22, PP. 74-78, 1975.

6. C.T. Tai, 'The effect of a grounded slab on the radiation from a line source', Journal of Applied Physics, Vol. 22, No.4, April 1951.

7. K.C. Gupta, 'Narrow-beam Antennas Using Artificial Dielectric Medium with Permitivity Less than Unity', Electronics Letters, Vol. 7, No. 1, PP.16-18, 1971.

8. T. Tamir, and O.A. Aliners 'The Influence of Complex Waves on the Radiation Field of a Slot-excited Plasma layer', IRE Trans. AP-10, PP. 82-95, 1962.

9. J.W. Duncan, 'The Efficiency of Excitation of a Surface Wave on a Dielectric Cylinder', IRE Trans., MTT-7, PP. 257-268, 1959.

10. R. Mitra and S.W. Lee, Analytical Techniques in the Theory of Guided Waves. The Macmillan Company, New York.

11. B.Noble, Methods based on the Weiner-Hopf Technique. Pergamon Press 1958.

12. C.P. Bates and R. Mittra, 'Waveguide Excitation of Dielectric and Plasma Slabs', Radio Sci., 3, No.3, PP. 251-266, 1968.

13. C.P. Bates, and R. Mittra, ' A Factorization Procedure for Weiner-Hopf Karnels 'IEEE Trans., AP-17, No. 1, PP 102-103, 1969.

14. E.C. Titchmarsh, A Theory of Functions, Oxford University Press, 1978.

15. W.R. LePage, Complex Varriables and the Laplace Transform for Engineers. Tata McGraw-Hill, Bombay.

16. E.O. Hammerstad, 'Equations for Microstrip Circuit Design', 5th. European Microwave Conf., PP 265-272, Sept. 1975.

17. R.F. Harrington, Time-Harmonic Electromagnetic Fields. McGraw-Hill, New York, 1961.

18.

EE-1981-M-GOG-EFF